공학박사 학위논문

High throughput nano-electrokinetic purifier for an artificial kidney

이온 공핍 영역의 불안정성 억제를 통한 전기수력학 장치의 수처리 용량 증대 및 인공 신장 시스템에의 적용

2018 년 8 월

서울대학교 대학원

전기 · 컴퓨터공학부

김 기 홍

High throughput

nano−electrokinetic purifier

for an artificial kidney

지도 교수 김 성 재

이 논문을 공학박사 학위논문으로 제출함
2018 년 7 월

서울대학교 대학원
전기 · 컴퓨터공학부
김 기 홍

김기홍의 공학박사 학위논문을 인준함
2018 년 7 월

위 원 장 홍 용 택 (인)

부위원장 김 성 재 (인)

위 원 김 호 영 (인)

위 원 성 건 용 (인)

위 원 곽 노 균 (인)

Abstract

High throughput nano-electrokinetic purifier for an artificial kidney

Kihong Kim

Department of Electrical and Computer Engineering

College of Engineering

The Graduate School

Seoul National University

After the recent development of perm selective membrane and nano-scale fabrication process, various electrokinetic methods for water treatment have been emerged. In case of these methods, ion concentration polarization (ICP) phenomenon has been extensively researched concerning new fundamentals in nanoscale electrokinetics and novel engineering applications. However,

effective platform for ICP device has not been sufficiently accomplished and the technique has suffered from the critical limitation of low processing capacity. In this thesis, microfluidic apparatuses were adapted to develop highly utilized ICP platform and micro-scale structure was installed the layer near the membrane to enhance throughput of ICP devices, respectively. And we finally invented the electrokinetic purification system for an artificial kidney system.

Firstly, we devised a new micro/nanofluidic preconcentrator using ICP phenomenon by integrating a two-phase droplet generator and pneumatic valve. One of the most interesting features of ICP is collecting any charged species at the interface between ICP layer and bulk electrolyte so that its concentration would be amplified more than 10,000 times within a minute. In order to prevent the unwanted diffusion of highly concentrated sample plug, a droplet generator was employed to capture the preconcentrated plug and finally we can keep the high amplification ratio in high throughput manner by tweaking electrical input, flow rate, and concentration/release time. In addition, we adapted pneumatic valve to continuous type ICP preconcentrator. Highly concentrated plug is released to opened branch by controlling pneumatic valve within 100 ms so that we can continuously gather only concentrated sample. Manipulation of amplification ratio is similar with ICP droplet preconcentrator which could be amplified more than 100 times.

Secondly, we devised micro fin structures inside a macroscale (>O(2) um) highthroughput ICP device and successfully demonstrated a stable formation of ICP layer and its performance. Since the fin structures created electroosmotic fluidic circumstances and assisted in physically suppressing undesirable electrokinetic vortices generated in this fluidic regime, ICP was stably generated even in this macroscale system. The micro fin structure was designed after proceeding analytical solution and numerical simulation. Finally, batch-type droplet ICP preconcentrator and continuous-type ICP separator were introduced as examples for high-throughput millimeter-scale ICP devices using the implanted fin structures.

Finally, we proposed high-throughput electrokinetic purification device for an artificial kidney system. Peritoneal dialysis (PD)-based wearable artificial kidney (WAK) device with portable and automate purification capability will provide dialysis treatment that has maximum freedom of time and space constraints for end stage renal disease (ESRD) patients compared to conventional PD or hemodialysis (HD) treatment. ICP phenomenon has been intensively attracted attention for portable purification applications because of extensive separation capabilities from ion to micro-scale substances by nanoelectrokinetic fundamental. In this work, nanoelectrokinetic purifier, for the first time, was applied for a portable PD device which can overcome several limitations of a conventional PD treatment. First of all, dialysate purification mechanism was verified using a micro-nanofluidic platform.

Uncharged toxin (urea) was completely decomposed to non-toxic gases (~99 % purified) by electrochemical reactions and positive toxin (creatinine) was sufficiently removed (~40 % purified) by nanoelectrokinetic transportation which is similar to the cation transport mechanism due to ICP phenomenon. And a macro-scale nanoelectrokinetic purifier (10 mL/min throughput) with a creation of micro-nanofluidic environment inside the device was successfully demonstrated as a dialysate purification device for continuous flow PD. As a result of extensive in-vitro and in-vivo experiments, the toxin level in a body fluid of the dog was verified to be reduced around 10 % during 3 hours of nanoelectrokinetic-PD treatment. One would expect the WAK for significantly advancing a quality of life for ESRD patients by this portable nanoelectrokinetic purifier.

Keywords : micro/nano fluidics, electrokinetics, ion concentration polarization, instability suppression, throughput enhancement, peritoneal dialysate recylcer

Student Number : 2013-20749

Contents

List of Figures

List of Tables

Chapter 1. Introduction

1.1 Research background

1.1.1 Perm selectivity of the nanochannels

All of materials in nature have their own surface charge. Therefore, when they contact with another material, especially air or liquids, form intrinsic charged layer which called electrical double layer (EDL) [1]. The number of theories about EDL has been studied since 1900, and it is now simply considered as figure 1.1. This model was developed by Louis Georges Guoy and David Leonard Chapman in 1910 and 1913 independently. The electrolytes in aquatic solution are redistributed depending on the both surface charge density of the wall and the concentration of solution. Counter ions of the surface charge consists the Stern layer near the wall and the free ions consists the diffuse layer. Concentration and electric potential of ions (solution of 1:1 electrolyte) are described by Poisson-Boltzmann equation as a function of distance from the wall [2].

$$\frac{d^2\psi}{dx^2} = \frac{en_0}{\epsilon_0\epsilon_d} \cdot \left[e^{\frac{-e\psi(x,y,z)}{k_BT}} - e^{\frac{e\psi(x,y,z)}{k_BT}} \right]$$

After redistribution at low potential wall, the EDL thickness is characterized by Debye length (λ_D**)** as

$$\lambda_D = \left(\frac{\epsilon_0\epsilon_d k_B T}{e^2 n_0} \right)^{0.5}$$

Where ϵ_0 and ϵ_d are permittivity of air and water, respectively, R is the gas constant, T is the absolute temperature, F is the Faraday constant, z is the

valance of ions and n_0 is the number of cations in the solution.

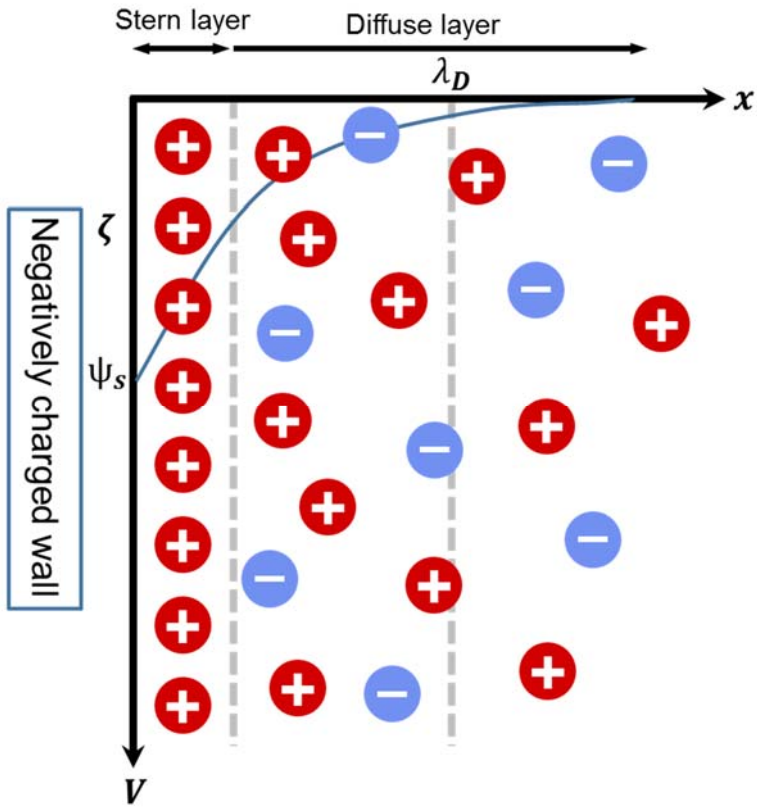

Figure 1.1. Schematic image of electrical double layer

The electric potential of bulk is not affected by EDL when the fluidic system is larger than microscale. However, if two walls are close enough (< *O(*2) nm), EDL of each wall starts to overlap and the electric potential of bulk becomes nonzero as figure 1.2. [3]. This state gives the perm selectivity to the nanochannel. Depending on the surface charge of the wall, whole area of nanochannel is charged with positive or negative value. Thus, every charged

species in the solution which have same sign with the wall are repelled from the nanochannel and not able to pass the channel. Recent advances of techniques using EDL and perm selectivity of nanochannel have provided a rigorous water-treatment platforms [4-8].

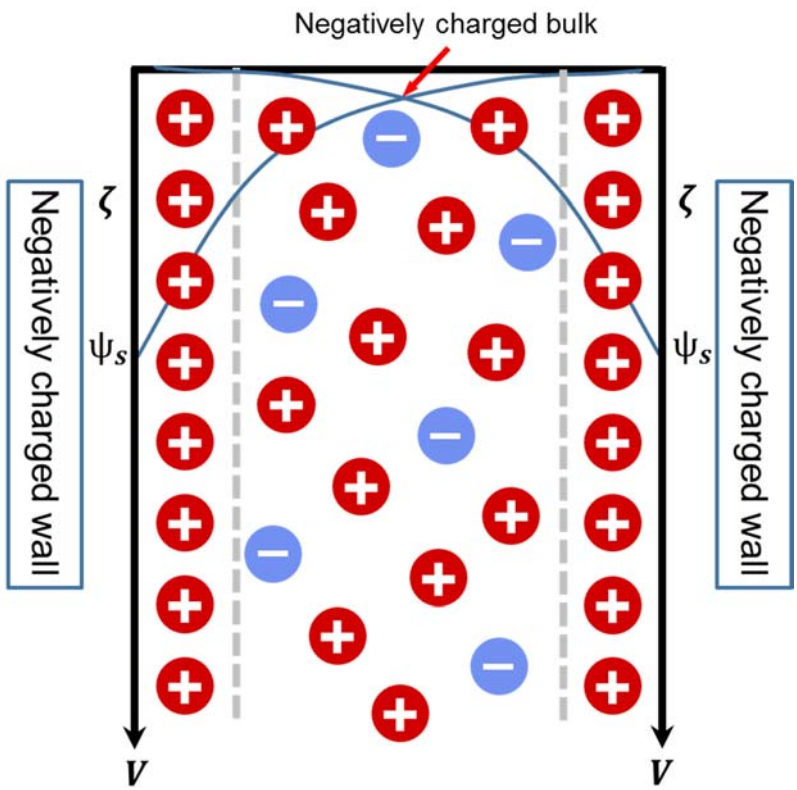

Figure 1.2. Schematic image of overlap of electrical double layer

1.1.2 Current techniques using nanochannels

Recent years, people have focused on the large-scale water treatment like reverse osmosis and thermal desalination. However, these methods have some issues-expensive facility costs, low power efficiency and environmental problems. Electrokinetic methods using perm-selective membranes are promising water treatment technique for resolve these limitations. Electrokinetic methods are bottom-up technique so that easy to control the size, throughput and power consumption of equipment.

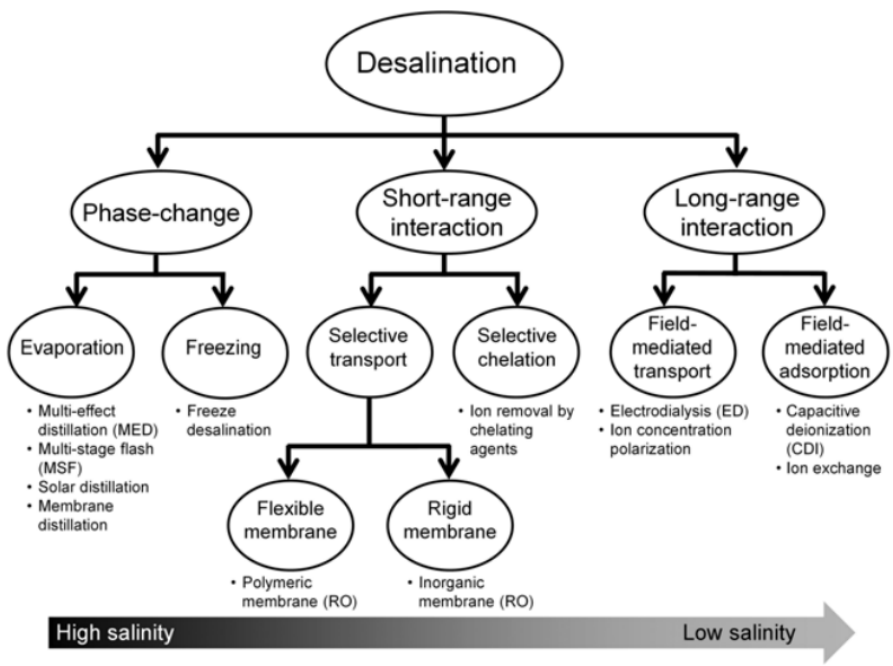

Figure 1.3. Overview of separation mechanisms and their use in desalination technologies [9]. Phase-change techniques are typically more suitable for high salinity water while field-mediated techniques are better suited for low salinity water.

Electrodialysis

Electrodialysis is the most popular electrokinetic method which uses perm selective membrane. Both cation exchange membrane (CEM) and anion exchange membrane (AEM) are used to eliminate cation and anion, respectively. Single cell of electrodialysis equipment is thinner than a millimeter and spacer is inserted to maintain specific channel thickness. Several single units are stacked with alternately arranged CEM/AEM so that desalted stream and highly concentrated stream are separately extracted after voltage applied as figure 1.4. The device operates at limiting current (typically voltage under 2 V) and the throughput is controlled by the number of cells [5, 10, 11].

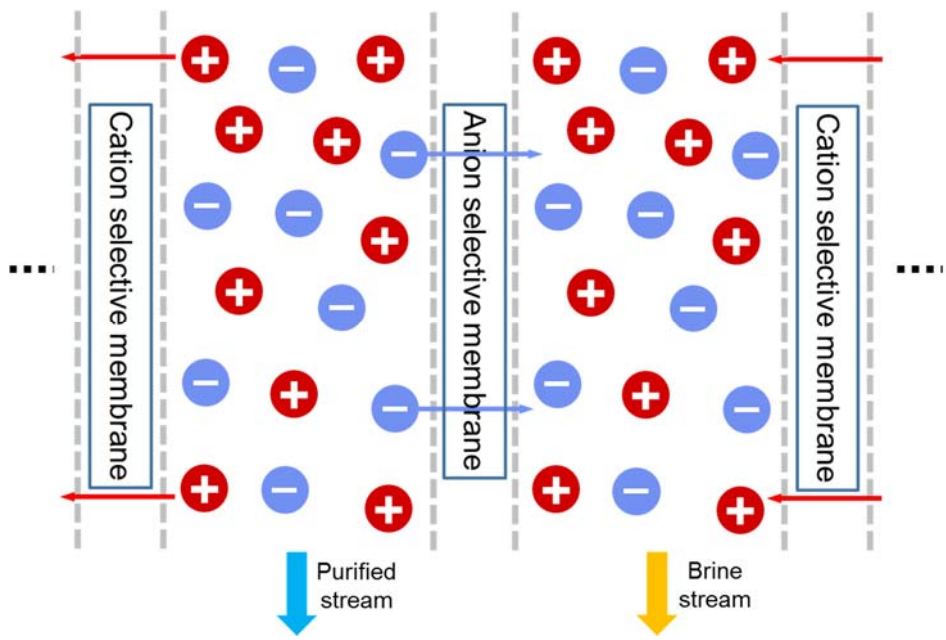

Figure 1.4. Schematic image of electrodialysis

Electrodeionization

Electrodialysis is difficult to purify ionic species clearly because purified stream becomes more electrically resistive at low concentration. Electrodeionization is developed to resolve this problem by adopting additive ion exchange resin which is filled between perm selective membranes. Additive ion exchange resin enhances ion transportation and purification efficiency over 50%. Various types of ion exchange resin have been developed beyond traditional beads model [6].

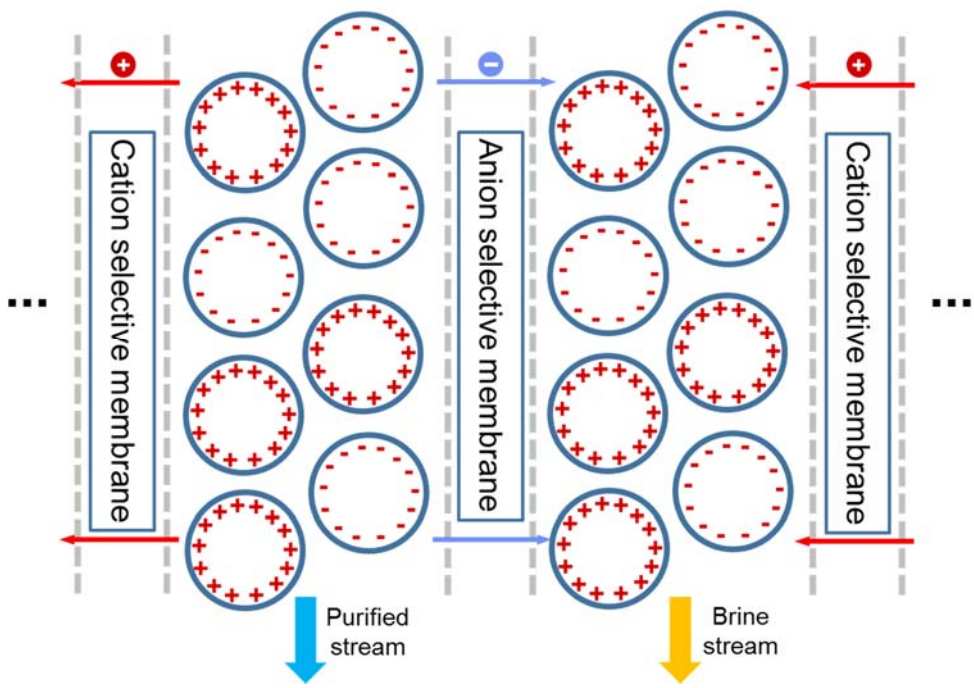

Figure 1.5. Schematic image of electrodeionization

Capacitive deionization

Capacitive deionization operates as the capacitor of ionic species. CDI system is consisted of the pair of microporous electrode. After voltage applied, ionic species in injected sample adsorbed to the EDL of micro pores. Absorbed ionic species are released when purification step finishes and the microporous electrode can be reused for purification. Recent researches are focused on enhancing the salt adsorption capacity and the lifespan/stability of microporous electrode [7, 12, 13].

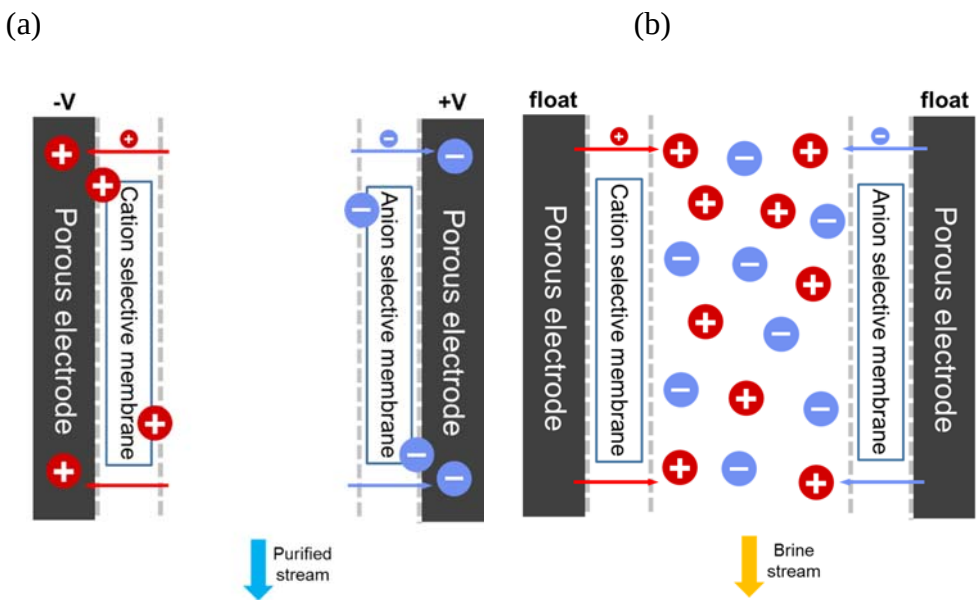

Figure 1.6. Schematic image of capacitive deionization; (a) deionization step (b) regeneration step.

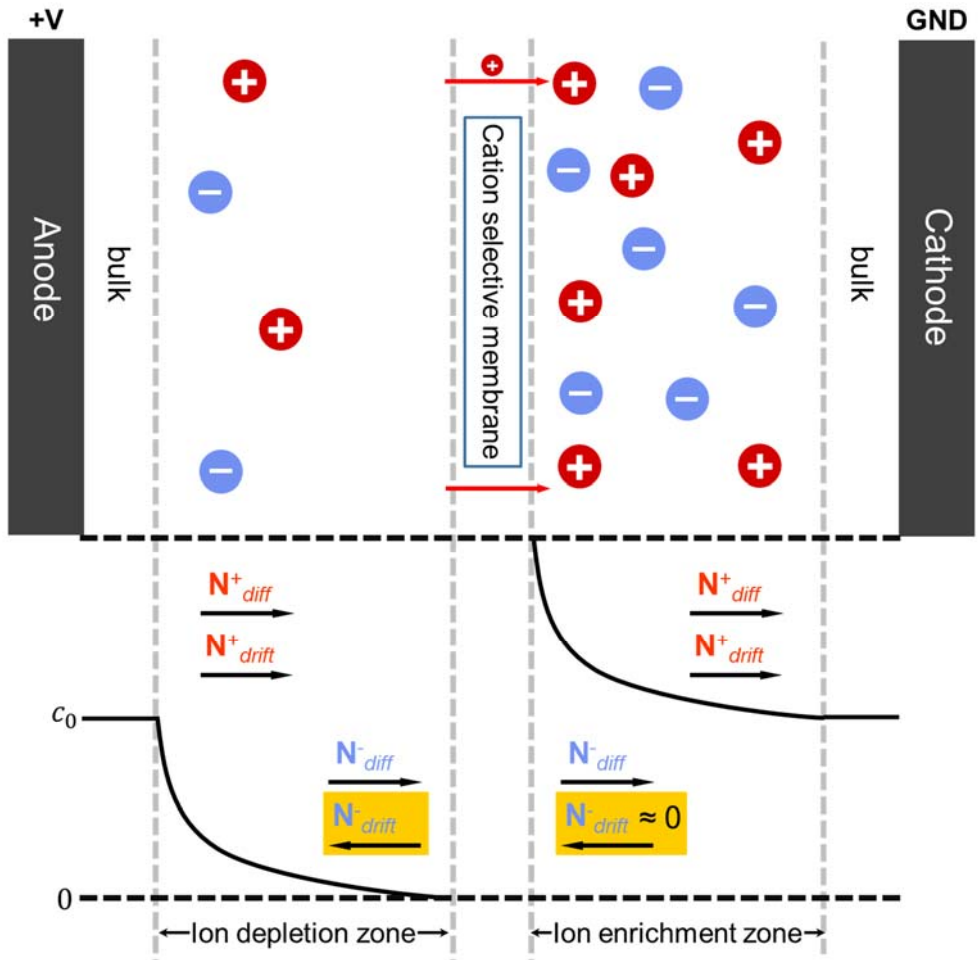

Figure 1.7. Schematic image of ion concentration polarization and concentration plot of ions.

1.1.3 Ion concentration polarization

Ion concentration polarization (ICP) phenomenon is microscopic observation of ion concentration profile near a perm selective membrane [8, 14]. The phenomenon is developed from research of ion transport mechanism, which is coupled multi-physics of convective diffusion and electric field. Typical ICP system is consisted of two electrodes with perm selective membrane (suppose as CEM) dividing it into two distinct area. When we apply electric field across the membrane, cations transport to another side and ion concentration is polarized as figure 1.7. The cathodic area near the membrane called ion depletion zone, and the opposite sited called ion enrichment zone. The desalinated water and brine could be extracted from ion depletion zone and ion enrichment zone, respectively. Furthermore, highly concentrated charged species could be gathered near the boundary of ion depletion zone [15, 16]. The transport mechanism of ionic species varies with the characteristic length of system, corresponding content will be dealt in chapter 3.

1.2 Thesis overview

ICP phenomenon has been studied from recent date (SJKIM) comparatively with other electrokinetic systems, because micro/nano fluidic system is difficult to fabricate the device and observe the behavior. Thus, there are not optimized platform for practical uses.

Firstly, the method to effectively handle desalinated and concentrated streams is insufficient. There are batch type [15, 17] and continuous type [16, 18] for existing operation methods, however, these methods have each difficulties for extraction and control of concentration ratio, respectively. These drawbacks could be resolved by applying microfluidic platforms which would be dealt in Chapter 2.

Secondly, regardless of pros and cons of device types, every microfluidic platform have significant technical drawbacks in low processing capacity which is highly demanded for practical applications. Scaling up by widening microchannel dimension destroys several benefits of micro/nano fluid mechanics such as laminar flow characteristics and independency from gravity. Most importantly, electrokinetic instability becomes severer with larger microchannel dimension [19-24]. After verification of electrokinetic instability near perm selectivity membrane by COMSOL simulation (Chapter 3) and experiments (Chapter 4), the instability was suppressed and ICP device successfully operated in high throughput condition.

Finally, we proposed a nanoelectrokinetic dialysate purification device for continuous flow peritoneal dialysis (PD). A micro-nanofluidic device was

employed to verify the mechanism of contaminant removal. An in-situ visualization and a direct chemical analysis demonstrated that anionic species in a used dialysate rerouted around the ion depletion zone and cationic species including creatinine in a used dialysate was mostly removed by cationic flux through the nanojunction. On the other hand, urea which is known for electrically neutral body toxin was electrochemically decomposed to gas bubbles at the anodic electrode. Therefore, we would continuously obtain a purified dialysate by extracting stream from the ion depletion zone. Finally, this micro-nanofluidic platform was scaled-up using commercial 3D printer. A microfluidic environment was created in this scaling-up device using a confined micro-geometry which prevented undesirable instability and enhanced the removal of cationic species. In-vitro experiment using a used dialysate obtained from patients who underwent PD and in-vivo experiment on canine model were conducted for verifying this new scheme.

Chapter 2. Electrokinetic preconcentration in micro-nanofluidic system

2.1 Introduction

The concentration of biomarkers in human body is also extremely low for trustworthy sensing in biosensor application field. Thus, the preconcentration of such low abundant samples can guarantee the commercial profit and suitable sensitivity.

Recent advances of nano fabrication techniques have provided a rigorous experimental platform to investigate novel ion transportation in nanofluidic system. Among them, Ion Concentration Polarization (ICP) phenomenon has been playing a key mechanism of various new engineering applications such as ion/protein preconcentrator and desalination, etc.

One of the most interesting features of ICP is collecting any charged species at the interface between ICP layer and bulk electrolyte so that its concentration would be amplified more than 10,000 times within a minute. Highly concentrated ionic plug can be generated by applying tangential field (either pressure or electric) to the ICP layer, typically called batch-type preconcentrator4. On the other hand, continuous-type preconcentrator used relatively high pressure field for separating desalted/concentrated streams on two outlet device. Both types had significant drawbacks in terms of instability and amplification ratio, respectively. In this presentation, we proposed a feed-batch type preconcentrator as shown in Figure 2.1 which hybridized the batch

type ICP preconcentrator with continuous droplet generator to overcome the drawbacks. On another approach, we focused on extraction of purified/concentrated stream from continuous type ICP separator. Pneumatic valve system has been utilized with several microfluidic platforms from 2000 [25]. We integrated pneumatic valve with continuous type ICP separator shown as figure 2.2.

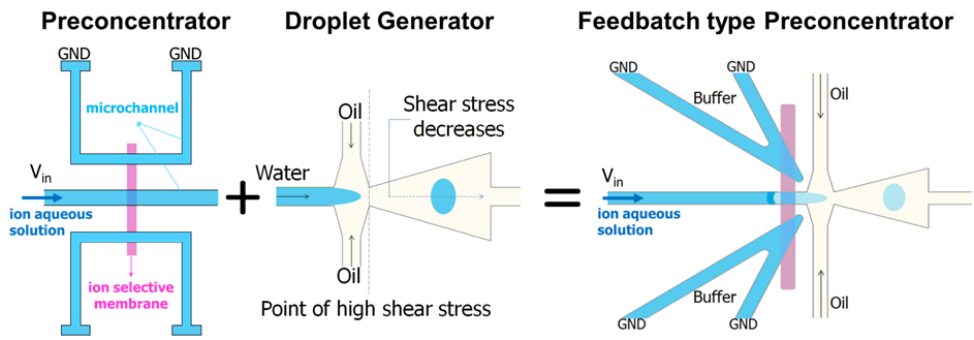

Figure 2.1. Schematic image of batch type preconcentrator integrated with droplet generator

(a) (b) (c)

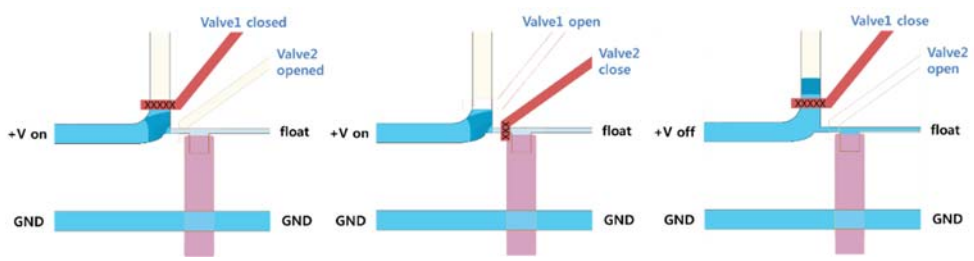

Figure 2.2. Schematic image of continuous type preconcentrator integrated with pneumatic valve system. (a) Concentrating (b) release (c) reset steps, respectively.

After integrated, only plugs containing highly amplified charged species are extracted to the upper branch by controlling two pneumatic valve channels following sequence.

2.2 Experimental section

Fabrication of droplet-integrated ICP preconcentrator

Polydimethylsiloxane(PDMS) molding and nafion patterning techniques are used to fabricate the device. First, SU-8 photoresist was patterned on silicon wafer and PDMS was molded with the wafer. Second, coat PDMS on glass and then nafion was patterned on this coated glass. After all, align and attach two systems by plasma bonding. Fabricated device is shown in figure 2.3.

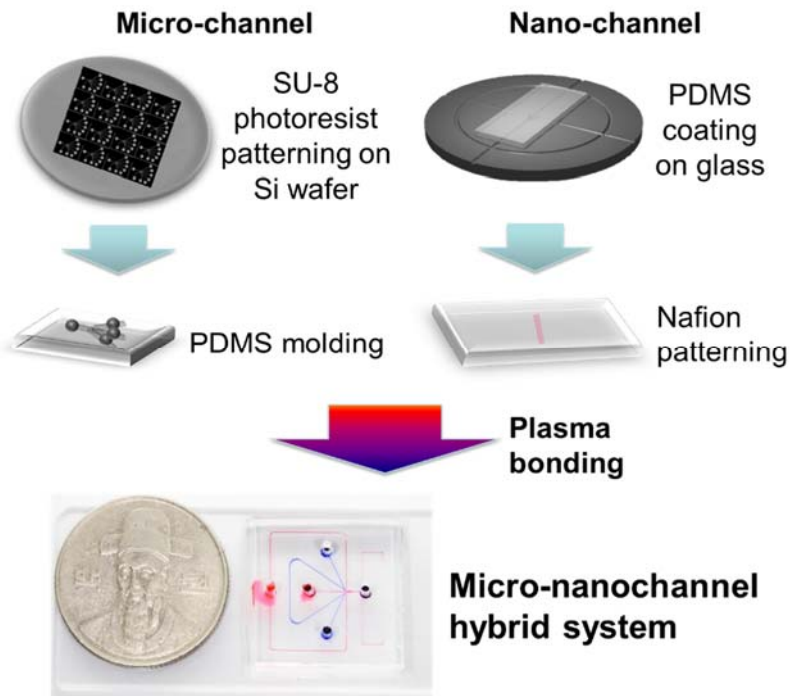

Figure 2.3. Fabrication of batch type preconcentrator integrated with

droplet generator

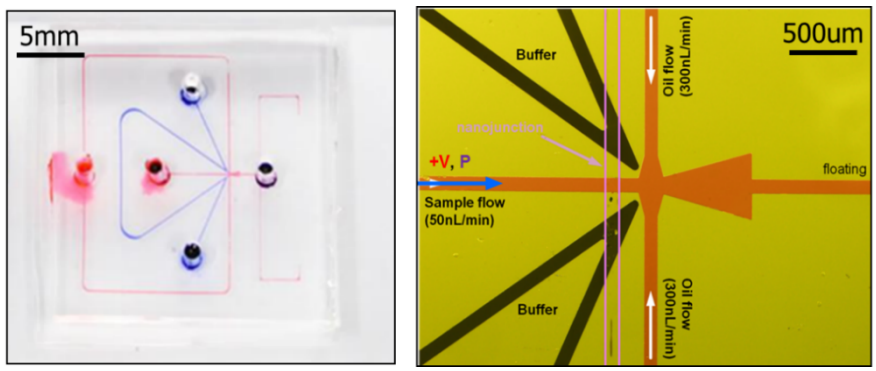

Figure 2.4. (a) The image of a device (b) Microscope image of the fabricated PDMS microchannels integrated with a surface patterned nanojunction

Fabrication of pneumatic valve-integrated ICP preconcentrator

Polydimethylsiloxane(PDMS) molding and nafion patterning techniques are used to fabricate the device. First, SU-8 photoresist of ICP operation channel and pneumatic valve channel were patterned on silicon wafers, respectively. Second, coat PDMS on ICP operation channel patterned silicon wafer and PDMS was thickly molded with pneumatic valve channel. Third, pneumatic valve channel was aligned and attached to ICP operation channel. Fourth, coat PDMS on glass and then pattern on nafion this coated glass. After all, align and attach two systems by plasma bonding. Fabricated device is shown in figure 2.4.

Experimental apparatus

Obtained data is analyzed by Labview program. 1mM KCL solution is used for aqueous phase and oleic acid is used for oil phase. Alexa-488 is used as fluorescent tracker. External pressure was applied by Harvard PHD2000 and electrical voltage was exerted by Keithley SMU-238.

2.3 Result and discussion

Droplet-integrated ICP preconcentrator

The operation consisted of 3 steps; initiation, concentration, and encapsulation. First, regular droplet whose concentration is the same as buffer sample is generated without external voltage (left image of figure 2.5). Next, anions and charged particles are started to be concentrated within a plug with external voltage and desalted droplets were generated as shown in middle image of figure 2.5. Turning off the voltage let highly concentrated plug be released and encapsulated in a droplet (right image of figure 2.5).

Enhanced concentration ratio is attained from measuring the fluorescent intensity. Measured plug concentration is about 50-folds, and encapsulated droplet concentration is more than 5-folds when average power usage is 2Wh/L. Specialty of this system is that concentration ratio and power usage can be controlled by arranging each operation step time and voltage.

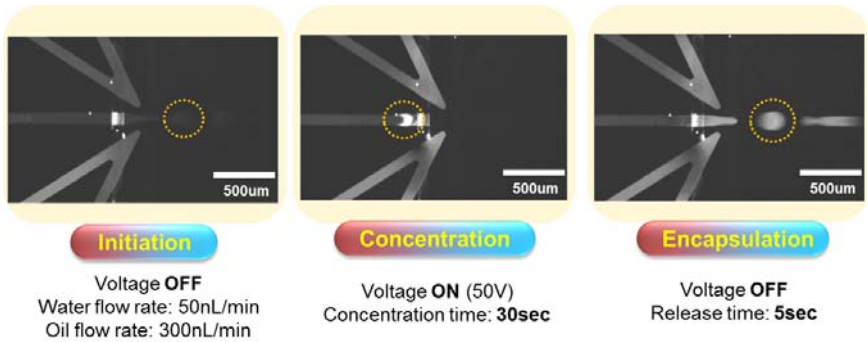

Figure 2.5. Image of 3-steps operation of droplet generator integrated preconcentrator

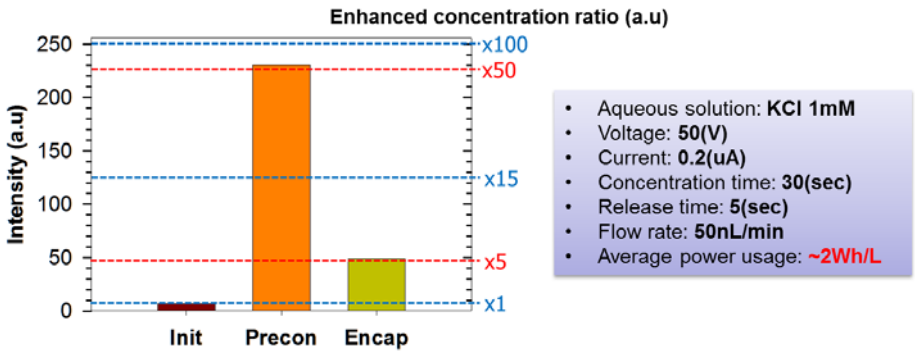

Figure 2.6. Experimental measurement of enhanced concentration ratio of the each step

Pneumatic valve-integrated ICP preconcentrator

The operation consisted of 3 steps; initiation, concentration, and releasement. First, regular sample flows to both upper/middle stream and buffer was injected to individual channel. (left image of Figure XX). Next, external voltage applied and upper valve is turned to close upper channel. In this step, anions and charged particles are started to be concentrated within a plug and desalted stream flowed to middle channel shown in middle image of Figure XX. Next, turning off the voltage and opening upper valve/closing middle valve. Then, highly concentrated plug is released to upper channel and middle valve is opened after a while (right image of Figure 3).

Enhanced concentration ratio is attained from measuring the fluorescent intensity. Measured plug concentration is about 100-folds, and the amplification of concentrated stream is more than 20-folds when average power usage is 2Wh/L. Even though pneumatic valve integrated system is s

slightly hard to fabricate than single layer microfluidic device, extremely highly concentrated sample could be achieved by adjusting operation step time without any post-processing.

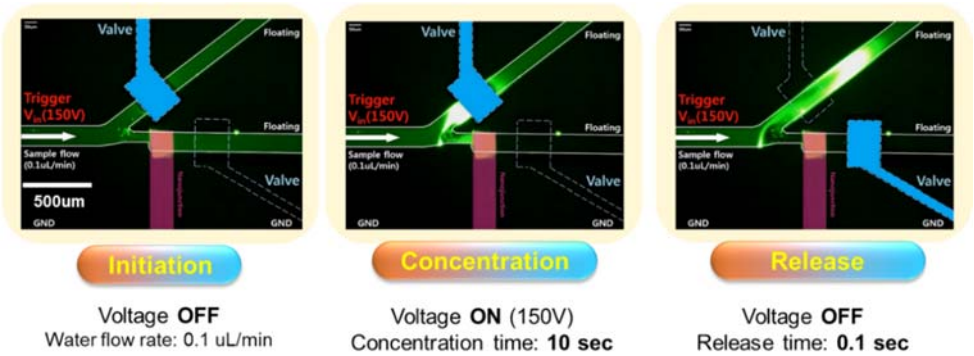

Figure 2.7. Image of 3-steps operation of pneumatic valve integrated preconcentrator

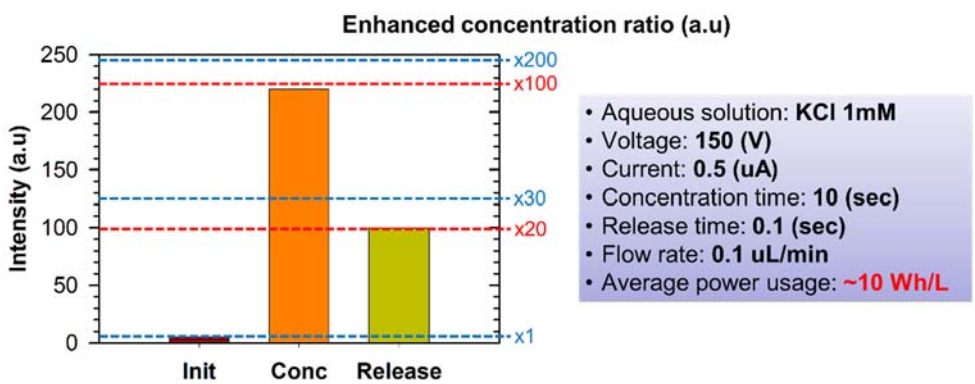

Figure 2.8. Experimental measurement of enhanced concentration ratio of the each step

2.4 Conclusions

While a nanofluidic preconcentration device has been actively developed for a decade, leverage between stability and amplification ratio still impeded commercial applications. Here we proposed that two types preconcentrator shows a great possibility to extract highly concentrated ions and charged species in micro-nanofluidic hybrid system in high throughput manner. Repeating each given operation steps of both types of preconcentrator effectively generated highly preconcentrated sample during the period of release time at minimum power consumption. In order to enhance the throughput, we build a multiplexed system, leading to increase several folds of processing capacity.

Chapter 3. Micro fin assisted massive parallelization of nanofluidic device

3.1 Introduction

For a last decade, the nanofluidics has been explosively researched about the development of new nanoelectrokinetics fundamentals as well as new engineering applications based on the fundamentals. Especially, a perm-selective ion transportation through a nanostructure has been regarded as a key field of nanofluidics [26-28]. The perm-selectivity (or ion-selectivity) refers an imbalanced ion transportation through the nanostructure (counter-ion more and co-ion less) [2]. While the origin of the selectivity has been debated until nowadays such as the overlapped electrical double layer (EDL) [17, 29, 30], new fundamentals and novel engineering applications utilizing the perm-selectivity opens several critical research fields. One of most exciting features was ion concentration polarization (ICP) [31]. ICP describes the polarization of ionic concentration near the nanoporous membrane (or nanochannel) under dc bias [14]. Typical behavior is that the concentration largely depleted at the anodic side of membrane and enriched at the cathodic side of membrane with cation-selective membrane such as Nafion [32]. The science behind the ICP such as the source of overlimiting current [14, 33-36] and electrokinetic instability [24, 37-40] has become the most attractive research field in nanofluidics and, moreover, the purification/desalination applications by the continuous extraction of fluid inside the ion depletion

zone has been drawn significant attention because this micro/nanofluidic platforms could be developed for a portable (or small scale) device which is essentially useful in remote settings [4, 8, 16, 41, 42]. In the meantime, one can utilize a brine stream of the purifier as well for developing molecular preconcentrators [31, 43-45]. These ICP preconcentrators enhance the limit of detection of any sensor for detecting low abundant samples such as cancer biomarkers and heavy metal substrates.

ICP purifier/preconcentrator has been successfully developed in the form of either batch type [15, 31] or continuous type [4, 16, 46]. Batch type device has higher preconcentration factor, but extracting the concentrated sample without losing the high amplification ratio was challenging [43, 47]. While continuous type device resolved the extraction problem, it has suffered from a lower preconcentration factor. Regardless of these detailed pros and cons, both types have significant technical drawbacks in low processing capacity which is highly demanded for practical applications.

Scaling up by widening microchannel dimension destroys several benefits of micro/nano fluid mechanics such as laminar flow characteristics and independency from gravity. Most importantly, electrokinetic instability becomes severer with larger microchannel dimension [19-24]. While shallower channel obviously brings out more stable ICP operation with surface conduction mechanism [34, 35], the dimension of microchannel should expand more than millimeter to obtain both practical throughput and easiness of fabrication. It has been reported that there were three main

(a)

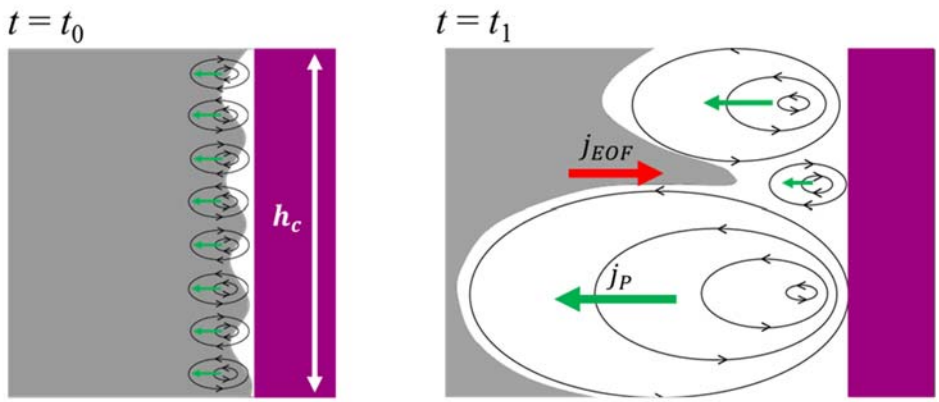

(b)

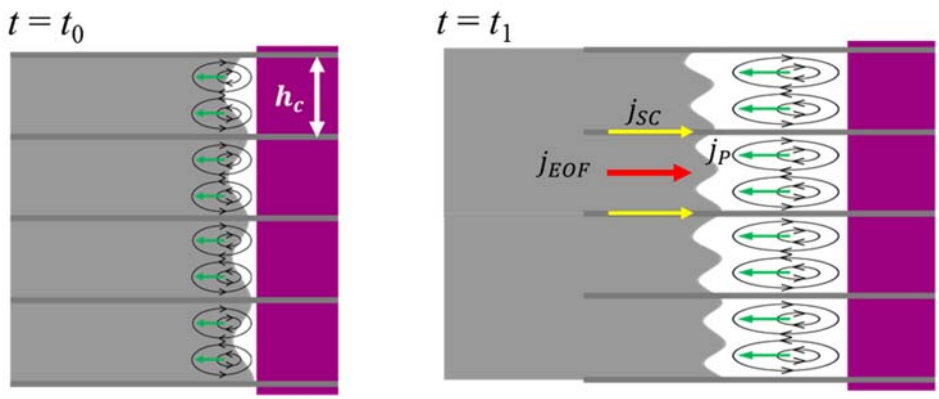

Figure 3.1. Schematics of vortex formation near perm-selective membrane (a) without and (b) with the micro fin structure. hc, jEOF and jP indicate the critical dimension, the ion flux by electroosmotic flow and back pressure due to vortex, respectively and, thus, the total flux would be jEOF + jP.

physical mechanisms that describe the limiting and overlimiting current of ICP phenomenon; surface conduction [34, 35], electro-convection[14, 48] and diffusioosmosis [33]. Surface conduction dominates in extremely narrow channels (<2um), while electro-osmotic flow (EOF) on the sidewalls

dominates in wider channels and transits to electrokinetic instability on the selective surface in very wide channels (>100 um) at the same channel depth. The sources of instability were the amplified electric field inside the ion depletion zone [49, 50] and ensuing strong vortical flow [23, 24]. Since the ion depletion zone has more than 100 times higher electrical resistance than bulk electrolyte, a large electric field drives strong electrokinetic vortices to satisfy the continuity conditions. The primary vortices are created in the vicinity of the nanoporous membrane and following secondary vortices arise, which merge to larger irregular vortices at the surface of the membrane as shown in Fig. 3.1 (a). However, primary vortices maintain their dimension, if the microstructure such as micro fin shown in Fig.3.1 (b) confines the critical dimension (h_c) of the microchannel as similar to the primary vortices. In this situation, the uneven and strong ion flux due to back pressure of vortex (j_P) would be regulated by the fin structure so that one is able to obtain more stable total ionic flux ($j_{EOF} + j_P$) along the fin structure. Therefore, one can accomplish both high-throughput and stable operation with the fin structure inside the ICP layer to suppress undesirable electrokinetic instability. Note that the surface conduction along the microchannel wall was negligible because the characteristic length scale of the system was 15 um. The surface conduction plays a dominant role when the characteristic length scale is less than 2 um [34, 35]. The basic design of the fin such as the critical dimension (h_c) and the length (l) was investigated as shown in Fig. 3.2 (a) and (b), respectively. The overlimiting conductance saturated as h_c decreased.

(a) (b)

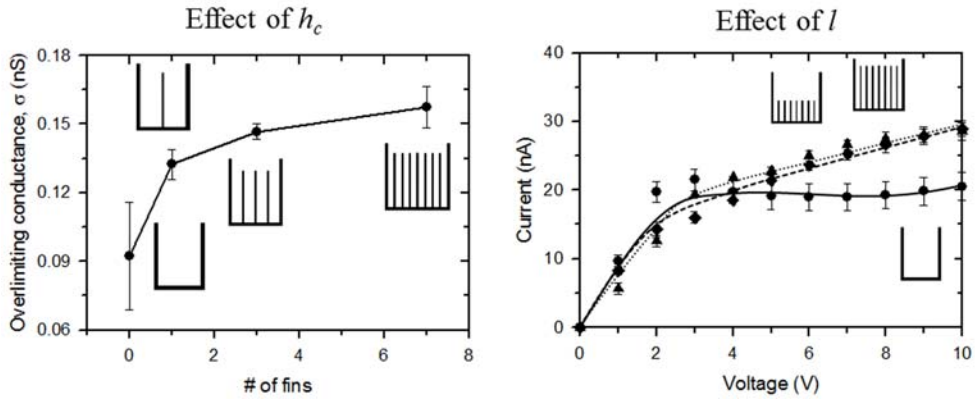

Figure 3.2. The effects of (a) h_c and (b) length (l) of fins are plotted.

Without the fin (h_c = 400 um), the conductance was a minimum due to the irregular ionic flux. As h_c become shorter, the fins were gradually capable of confining the primary vortices so that one can choose the number of fins near the location where the saturation behavior started. Also, the effect of fin length was investigated. Identical overlimiting current was obtained when the length of fin exceeded the dimension of primary vortices. In this work, we designed the fin structures (h_c = 100 um and *l* was varied as needed) in the macrochannel so that it was divided into several microchannels. It was a simple idea, but it suppressed the growth of vortices and the electrokinetic instability by the aforementioned scenario. The fin structure also allowed one to expand the width of the macrochannel at one's discretion, which directly enhanced the throughput of ICP devices. We applied the fin structures to a feed-batch type droplet ICP preconcentrator and continuous type ICP

separator and successfully demonstrated instability suppression and high throughput with the expanded dimension of the main channel over $O(1)$ cm.

3.2 Experimental section

Design of fin installed dual gate device

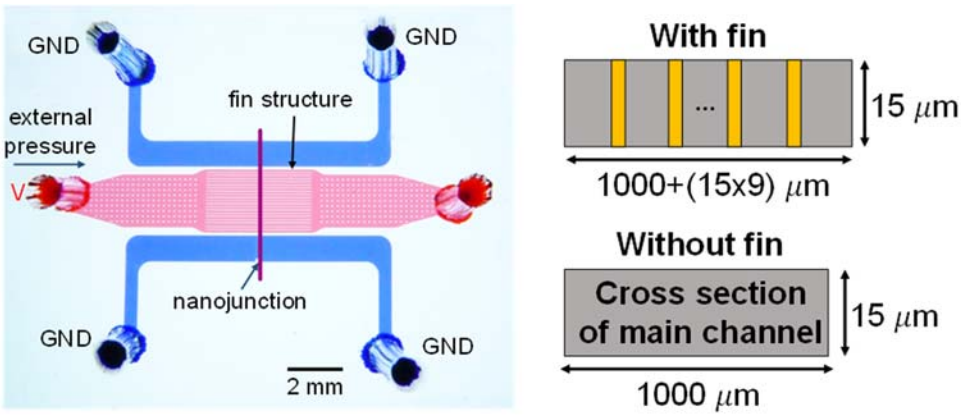

Figure 3.3. Representative image of fin-installed dual-gate ICP device. A schematic of the design of the fin structure is also shown.

Fin installed dual gated device was designed as shown in Figure 3.3. It consisted of one main microchannel and two buffer microchannels and they were connected with Nafion membrane. The membrane vertically patterned across the microchannels [51]. Dual gate device had two openings toward each buffer microchannel so that it assisted a sufficient and symmetric ion transportation. The width and spacing of fin was set to be 15 um and 100 um, respectively, with fixed microchannel depth of 15 um. The width of main microchannel was varied to 0.2, 0.5, 1, 2 mm with maintaining same increment ratio of cross sectional area for investigating the role of fin structures in a different geometry. The width and depth of both buffer microchannels was fixed to 1 mm and 15 um, respectively. Additionally, the

length of the fins were modified to lead equal concentrating position by balancing pressure distribution with desalination shock from nanojunction.

Preparation of poly(dimethylsiloxane) (PDMS) microchips

SU-8 2015 photoresist (MicroChem. Inc, USA) was spun on a 4-inch wafer to coat 15 um layer (at 500 rpm of 10 seconds (pre-spinning) and at 3250 rpm for 30 seconds (spinning)). After 3 minutes of soft bake at 95 ^{o}C, the layer was exposed two times to ultraviolet (UV) of 365 nm wavelength for 23.3 seconds (400 mW) using a mask aligner. The wafer was post-baked for 4 minutes at 95 ^{o}C, then was soaked in developer for 3 minutes. After rinsing with isopropyl alcohol and deionized water, trichloro (1,1,2,2-perfluoroocytl) silane (Sigma aldrich) was applied to the master wafer with a vacuum assisted deposition desiccator for easy detachment of the PDMS device.

PDMS base and curing agent (Sylgard 184 Silicone elastomer kit, Dow Corning, USA) were mixed at 10:1 ratio and desiccated in a vacuum pump for 1 hour to remove air bubbles. The mixed solution was poured onto the master and heated at 75 ^{o}C for 4 hours. The PDMS replicas were then peeled off from the master and the inlet and outlet holes were punched out.

A polymeric nanopourous material, Nafion (20 wt. % resin, Sigma Aldrich, USA), was used for the nanojunction between the microchannels. A single strip of Nafion (400 um wide and 1 cm long) was patterned on a slide glass using a PDMS piece that has a single straight microchannel and was heated at 95 C^{o} for evaporating solvent after removing the PDMS piece. Then, each

layer was bonded to the Nafion patterned slide glass by oxygen plasma bonder (Femto Science, Korea) under an alignment through the stereo microscope (SZ61, Olympus, Japan) creating a device. Final assembled ICP device is shown in Figure 3.3.

Materials and reagents

For both main channel and buffer channel solution, 1 mM KCl solution (Sigma Aldrich, USA) was mainly used with Alexa Fluor 488 fluorescent dye (0.90 uM, Invitrogen, USA). Since the ICP operation became unstable when higher salinity sample was used, 100 mM KCl solution was used for the instability test. For droplet preconcentrator demonstration, oleic acid were used for oil phase.

Experimental methods

Chemical samples were loaded into the buffer microchannel by applying instant positive pressure from each inlet reservoir. For the ICP droplet preconcentrator and ICP separator, external pressures were constantly applied from the main channel and the oil channel by syringe pump (PHD2000, Harvard Apparatus, USA). Ag/AgCl electrodes were inserted into the inlet and buffer reservoirs on the device and connected to a power supply (Keithley 6517 and Keithley 238, Keithley Instruments, USA), while the reservoir of the buffer channel was grounded. The motions of fluorescent dyes were tracked by an inverted fluorescence microscope (IX53, Olympus, Japan) and

recorded by CellSens (Olympus, Japan) computer program. Labview (2014, National Instrument) was used to obtain and analyze data.

(a)

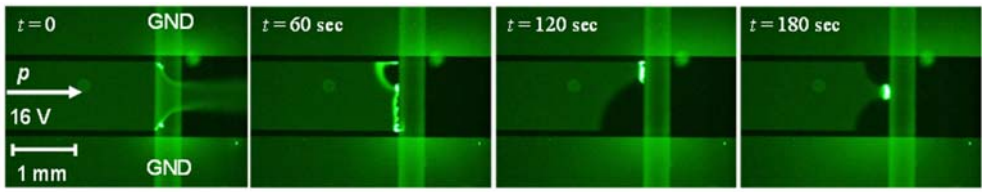

(b)

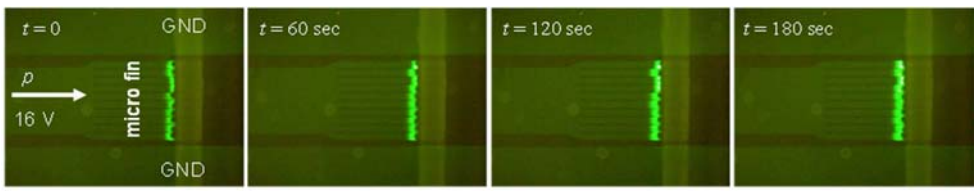

Figure 3.4. Time-evolving microscopic images of ICP formation in dual-gate device (a) without and (b) with the micro fin structure show that the fin was able to stabilize the ICP. The total widths of both channels were 1 mm.

3.3 Result and discussion

Basic ICP operation with fin structures

While typical ICP operation had been usually conducted only with an external electric field at early developing stage of ICP technology, the combination with an external pressure field provided various versatile functions to the typical ICP operation such as feed-batch type preconcentrator and electro-fluidic desalination device. However, the additional force by the external pressure field exerted to the electrical barrier which is the most important feature of ICP technology, leading to the destruction of the barrier and the unstable ICP operation. This instability became severer and all advantage of ICP technology would be diminished when the characteristic length scale exceeded micrometer scale. In order to conduct high-throughput ICP operation, however, the stable operation in a macrochannel (length scale over $O(1)$ mm) would be critical so that the fin structure in this work would play critical role to regulate the stability. ICP operations in millimeter scale channel without and with the fin structure were shown in Figure 3.4 (a) and Figure 3.4 (b), respectively. See the supporting videos as well. The width of main channel was fixed at 1mm and the external pressure field (linear velocity was 44 um/sec) was applied through the main channel. The external voltage (16 V) was applied at the left side of main channel, while the right side of main channel was floated. The electric field across the nanojunction generated the ion depletion zone (black area) out of background fluorescent dye (green area) and the dye was able to inform the status of the ion

(a)

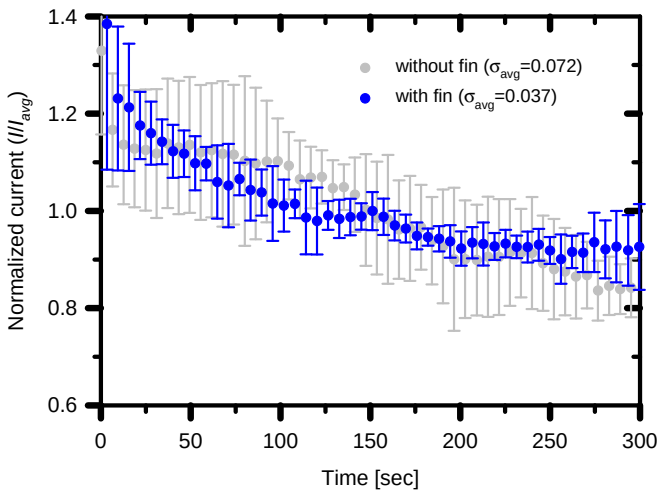

(b)

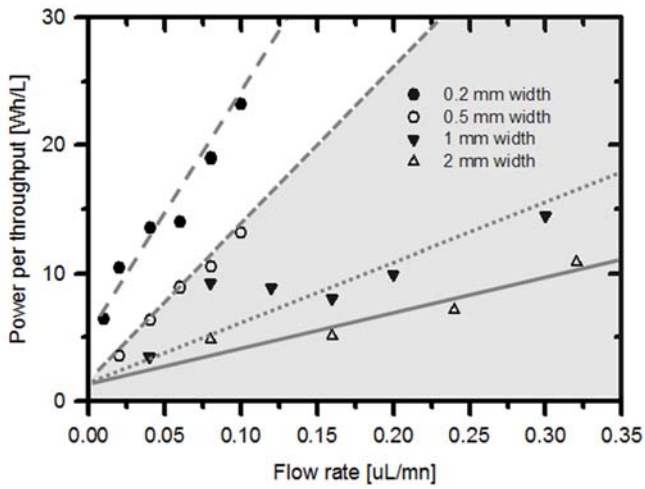

Figure 3.5. (a) I-t plots without and with the micro fin structure, showing the fin was also able to stabilize the ionic current (smaller standard deviation). The width of microchannel was 1 mm. (b) Plot of flow rate vs. power consumption. The grey area was only achievable with the micro fin structure

depletion zone. As shown in Figure 3.4 (a), the ion depletion zone inside the regular macrochannel (*i.e.* without fin structure) involved a repeated and fluctuated vortices, leading to undesirable leakages of accumulated dye at the boundary of the ion depletion zone. This would critically affect to the performance of nanofluidic preconcentration device. However, the ion depletion zone inside the fin installed macrochannel was stably formed and the dye was also uniformly accumulated at the boundary of the zone as shown in Figure 3.4 (b). This difference was quantitatively compared by measuring electrical current as a function of time in two platforms shown in Figure 3.5 (a). Standard deviations from the averaged value were 0.072 and 0.037 in the regular macrochannel and the fin installed channel, respectively. From these results, we concluded that fin structures would play an essential role of suppressing both fluidic and electric instabilities by creating microfluidic circumstances in the millimeter scale fluidic channel.

Moreover, the fin structures assisted to enhance not only the throughput but also the power efficiency as shown in Figure 3.5 (b). The power consumption was calculated by electrical current times applied voltage divided by the flow rate. The points in grey area of Figure 3.5 (b) was achievable only with the fin installed macrochannel. ICP operation failed without fin structure (no dye accumulation or severe leakage). The plot showed that (i) the relationship between the power consumption and the flow rate (*i.e.* throughput) was linear and (ii) the ICP operation consumed less energy in larger macrochannel (*i.e.* the power consumption became insensitive with larger macrochannel).

Dissipated energy due to exaggerated unstable fluid motion was saved by the regulatory function of the fin structure. Therefore, one can conclude that the fin structures would assist to suppress the electrokinetic instability and to enhance the throughput and the power efficiency simultaneously. Following sections would demonstrate these key roles of the fin structures in the practical millimeter scale ICP devices.

Fin installed droplet ICP preconcentrator

The first engineering application of ICP technology had been a biomolecular preconcentration device in the year of 2005 [52]. Compared to the other preconcentration schemes such as conventional filter, centrifugal separation, isotachophoresis [53, 54] and field amplified stacking method [55, 56], ICP preconcentration device has higher preconcentration factor because the biomolecules was able to be continuously injected through a microchannel and the ion depletion zone captured the molecules without leakage so that one can achieve a preconcentration factor up to million fold. However, extracting the preconcentrated molecules without loss had been highly challenging nuisance and several engineering endeavors were reported for efficient extraction methods such as onsite binding method [15, 57], integration with pneumatic valves [43] and micro encapsulations [47], *etc*. Among these techniques, encapsulating the preconcentrated molecule using two phase micro-droplet generator would be a versatile mechanism due to the easiness of integration with downstream analyzer, but generating larger droplet greater

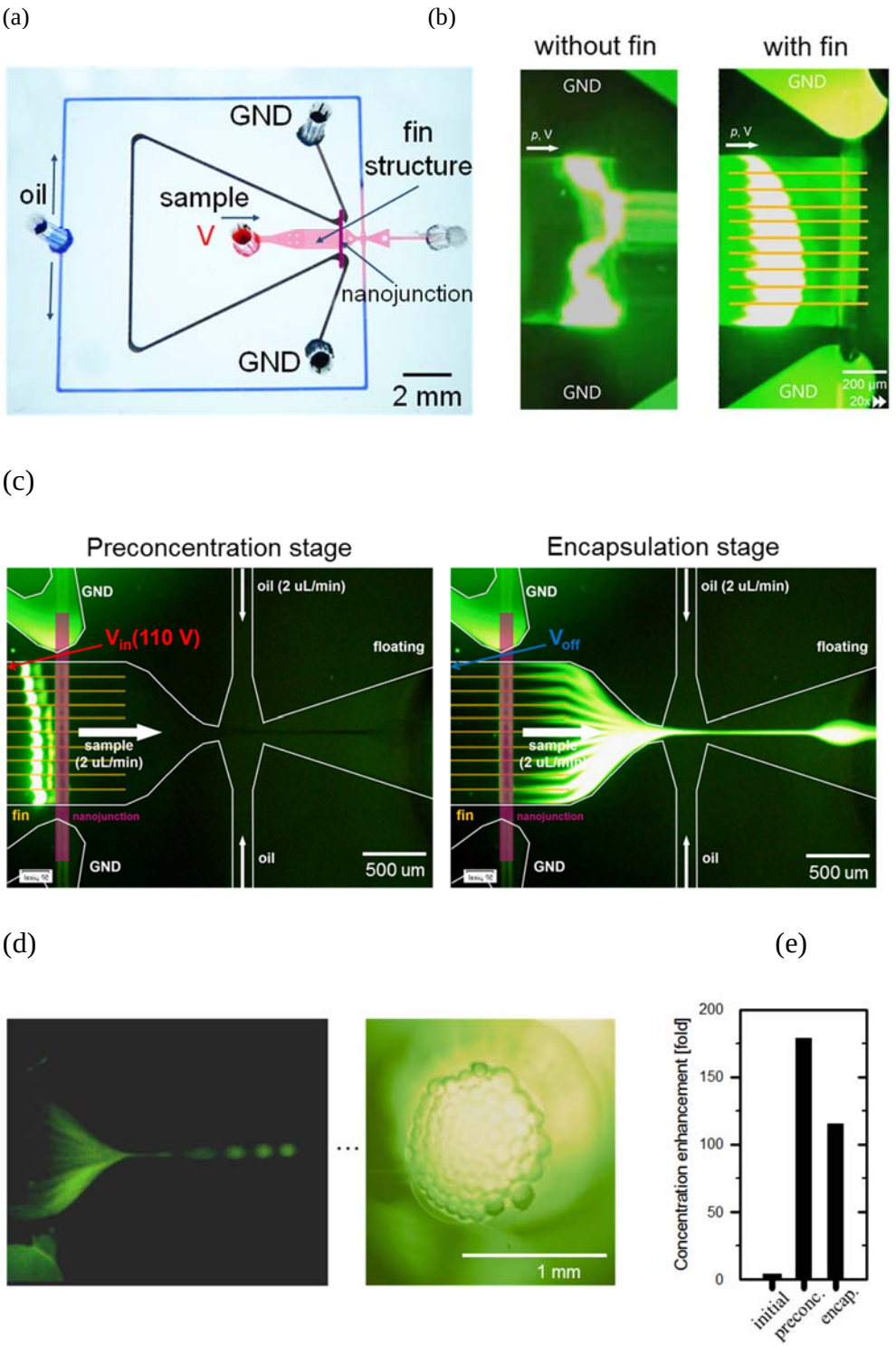

Figure 3.6. (a) A microscopic image of high-throughput ICP droplet generator. (b) Demonstration of the device without and with the micro fin

structure. (c) The operation process of fin-installed ICP droplet generator (preconcentration stage and encapsulation stage). (d) Microscopic image of encapsulated droplets of preconcentrated sample. Their diameter was more than 200 μm. (e) The preconcentration enhancement at preconcentration stage and encapsulation stage.

than 100 um of diameter often demanded for the electro-wetting-on-demand application, *etc*.

Figure 3.6 (a) showed an assembled photo of fin installed droplet ICP preconcentrator. The device consisted with three microchannels for disperse oil microchannel (blue), the main ICP microchannel (red) and the buffer microchannel (black). Oleic acid flew through the disperse oil microchannel from single inlet to the bottleneck which connected with the main ICP microchannel. Then the high shear stress at the bottleneck would cut the aqueous phase for generating the aqueous droplets of highly preconcentrated samples. A perm-selective nanojunction was positioned in front of the bottleneck and the electrical voltages were applied to the inlet of the main microchannel with the continuous injection of the sample, while the outlet of the main microchannel was floated and the buffer microchannel was grounded. Oleic acid was also injected through the oil microchannel during the entire process. The operation of the droplet ICP preconcentrator was two stage process. The first stage was a preconcentration stage (voltage on). Injected samples were preconcentrated near the nanojunction in this stage and

aqueous droplets were dispersed only with desalted water inside. The second stage was an encapsulation stage (voltage off). Preconcentrated plugs in the first stage were released toward the bottleneck because the electric field was removed. Then the encapsulated droplet would capture highly preconcentrated samples. Since unwanted diffusion across aqueous to oil phase was prevented, preconcentration ratio obtained in the first stage would be maintained also in the second stage. Here we installed the fin structures in front of the nanojunction to investigate their effects for the electrokinetic stabilization and larger droplet generation.

Figure 3.6 (b) showed a role of fin structures in a millimeter scale macrochannel at the first preconcentration stage. See the supporting videos for each operation. The applied voltage and flow rate in this demonstration were 40 V and 1 uL/min. While the plug fluctuated and the same severely leaked across the nanojunction without the fin structure, the preconcentration was stably established with the fin structure. Since there was a pressure field across the main channel, the shape of preconcentrated plug was parabolic.

The ICP droplet preconcentration process was demonstrated as shown in Figure 3.6 (c). At the concentrating stage with fin structure, stable preconcentrated plug was formed in front of the nanojunction without any leakages as shown in Figure 3.6 (c). As preconcentrating stage was maintained, the amplification ratio and the volume of plug were simultaneously increased. Note that the shape of plugs straightly aligned because the spaces between each fin was designed to prevent the parabolic

pressure field profile, leading to more uniform encapsulation. Concentrated sample was released as soon as turning off the voltage in a flash and flown toward the bottleneck. Then, the preconcentrated sample was captured by the oil inflow as shown in Figure 3.6 (d). The observation of encapsulated droplet was analyzed by a high speed camera (CASIO, EX-FC200S, Japan). After applying voltage for 50 sec, the peak concentration of sample was 180 folds at the preconcentrating stage, and the peak concentration of encapsulated 36 droplets enhanced 115 folds (Figure 3.6 (e)).The factor in the encapsulation stage was less than one in the preconcentration stage because the small portion of depleted sample should encapsulated as well, but optimizing the bottleneck structure would minimize the unwanted mixing. Additionally, the operation with a macrochannel over 1 cm width was also successfully demonstrated.

Fin installed continuous ICP separator

Similarly, the fin structures were also applicable for a continuous type ICP separator. The continuous type ICP separator was utilized in electro-desalinator [4] and continuous biomolecular preconcentrator [16] as well. While the preconcentration factor was limited by the dimensional ratio of bifurcated microchannels, the sample in a purified stream largely desalted over 100 times in both applications so that ICP separator was more useful for the desalination / purification applications than the preconcentration applications. The combination of external flow which was capable of bursting

the ion depletion zone would be the key mechanism of ICP separator [4, 49]. Any charged species flown through the main microchannel was vertically (upwardly) repelled from the nanoporous membrane so that their path would be deflected toward the upper brine microchannel. In these operations, high-throughput sample collection would be essential for further practical development.

(a)

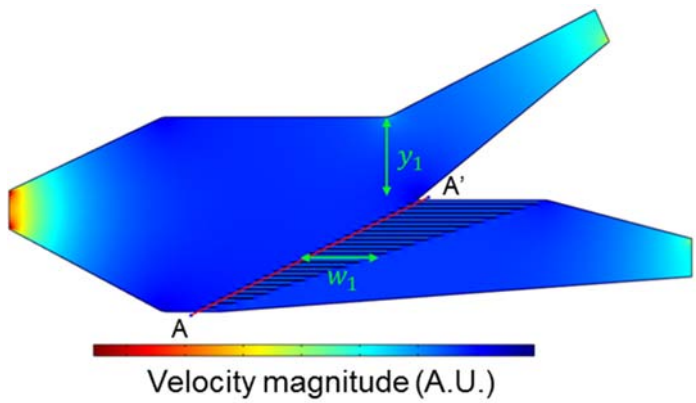

(b) (c)

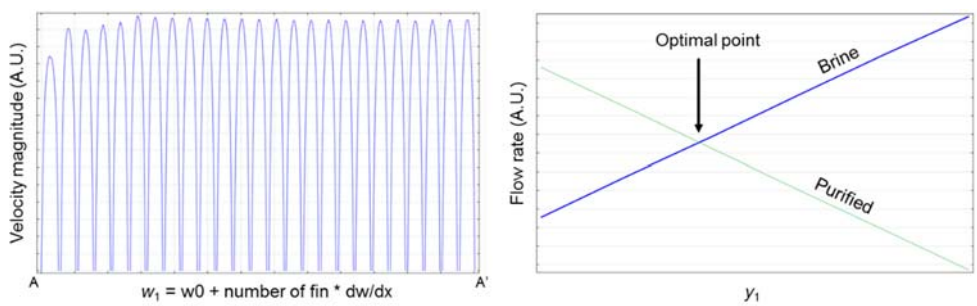

Figure 3.7. (a) Schematics of continuous ICP separator and the pressure field inside the device with fin structure. (b) The magnitude of velocity field along A-A', showing a series of parabolic profile in between each fin. Uniform

pressure distribution was obtained by adjusting the length of each fin. (c) The flow rates of brine stream and purified stream. The equal division was obtained by arranging y_1. The cross sectional area of purified channel with fin structure was the same to the one of the device without fin structure.

Numerical simulation was conducted using COMSOL Multiphysics. The numerical domain was depicted in figure 3.7 (a) and the pressure field, velocity field and flow rate was obtained using fluid dynamics module. No slip condition was assigned in physical wall. Inlet had constant flow rate condition and outlet had no viscous stress condition. w1 and y1 were adjusted to have the same fluidic resistance in between each fin (figure 3.7 (b)) and the equal division of input flow rate (figure 3.7 (c)), respectively.

A fin installed ICP separator was shown in Figure 3.8 (a). The main microchannel (red) had the dimension of 5 mm width and 15 um depth before the bifurcated point. By the serially-varied length of fin structures, the brine and the purified channel was designed to have the same fluidic resistance based on numerical simulation results. Consequently, an interval between each fin was set to be 100 um and lengths of them were gradually increased from a bottom-most fin to a top-most fin to regulate the pressure field. The nanoporous membrane was slantly patterned to assist the upward migration of charged species. The sample (KCl 1 mM) was continuously injected from the inlet of main microchannel (Q = 4 uL/min) with an electrical voltage (110 V).

(a)

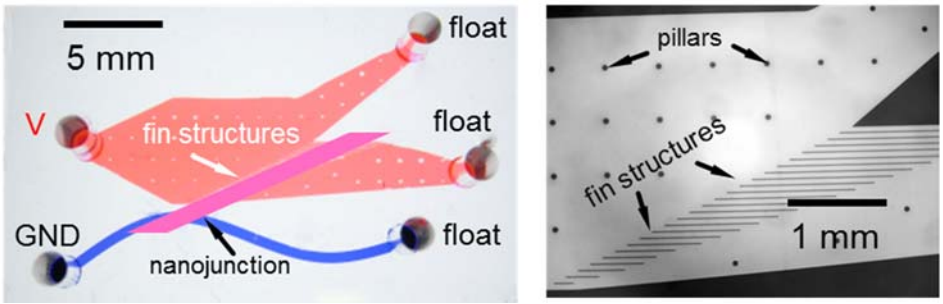

(b)

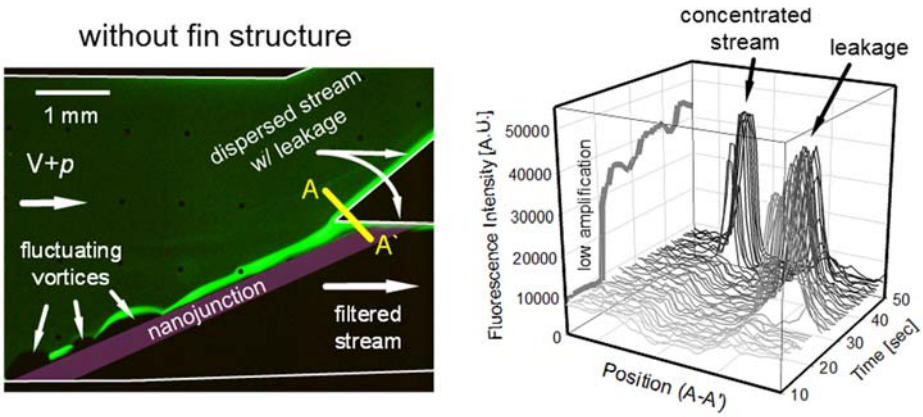

(c)

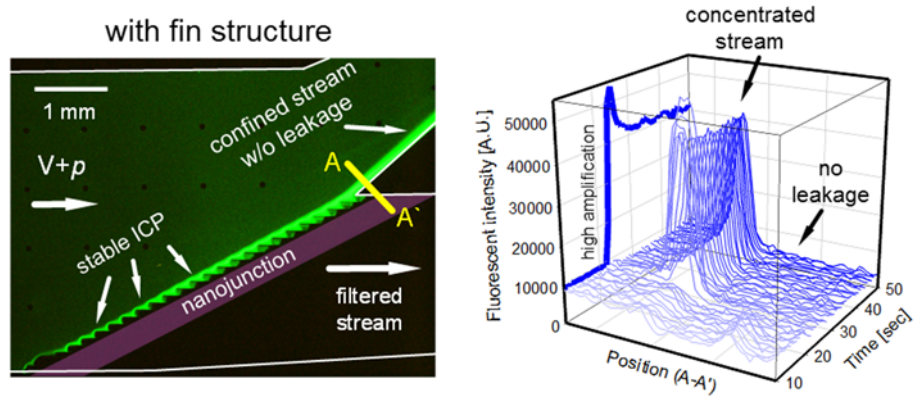

Figure 3.8. (a) A microscopic image of high-throughput continuous ICP separator and magnified image near the fin structure. A pillar array was installed to prevent the collapse of PDMS. Microscopic snapshots of the

filtration process (b) without and (c) with the micro fin structure and the corresponding fluorescence intensity plots, showing the fin structure was able to achieve higher concentration enhancement and less fluctuation.

Two outlet reservoirs were floated and the buffer microchannel was grounded. Figure 3.8 (b) showed that unstably formed fluctuating plugs along the nanojunction in a millimeter scale macrochannel without fin structures. This was because multiple random vortexes vigorously fluctuated back and forth, leading to dispersed preconcentration stream and leakages which should result in low purification (or preconcentration) ratio. Compared to this unstable operation, however, the fin assisted macrochannel had a quiescent ICP operation which resulted in narrowly defined preconcentration stream as shown in figure 3.8 (c), confirming the important role of fin structure. 3-dimensional plots in figure 3.8 (b) and figure 3.8 (c) would verify the progression of the filtration (or preconcentration) process. Fluorescence intensity of concentrated stream was measured in time-revolving manner to confirm that the fin structure assisted to efficient filtration (or rapid preconcentration) and stabilization of the stream, *i.e.* shaper increase and no fluctuation with the fin structure by comparing grey and blue solid line. The values of maximum fluorescent intensity at each time-span were choose to plot the lines in *x*-*z* plane.

3.4 Conclusions

Recently developed ICP technologies had been explosively researched because new physical aspect and its novel applications such as biomolecular preconcentrator and electro-desalinator. The major hurdle hindered the further development had been the low throughput due to microscale platform and the instability due to amplified electrokinetic field. Here we proposed the fin structures which were experimentally proven to be an appropriate remedy of such limitations. The structure would physically trap the instability which come from the scaling-up the channel dimension. While the throughput in this work was still questionable for commercial products, the presenting microstructure would play a key role for the massive parallelization even in 3-dimensional platform.

Chapter 4. High-throughput nanoelectrokinetic purifier for a practical peritoneal dialysate recycle

4.1 Introduction

End stage renal disease (ESRD) is a state of permanent failure of kidney with high risk of morbidity and mortality. Worldwide population of ESRD patients are sharply increasing at a rate of 5-7 % per year [58] giving rise to increased economic burden. Even with proper dialysis treatment, however, they are exposed to 30 times higher cardiovascular mortality than general population [59]. Adjusted mortality rates of ESRD patients amounted to 136 per 1,000 patient-years in recent USRDS annual report [60]. Moreover, Medicare Expenditures in for ESRD patients records the highest medical costs per patient among the other chronic diseases. For example, it amounted to be 30.9 billion dollars in USA, 2013.Patients with ESRD should choose a therapeutic modality among kidney transplantation, hemodialysis (HD), or peritoneal dialysis (PD). Kidney transplantation is the treatment of choice by virtue of best survival rate [61-63], optimal quality of life as well as cost utility [64-66], although problem of donor scarcity remains to be solved. Most ESRD patients without altruistic donor candidates should maintain HD or PD. The selection of dialysis modality depends on patient's medical conditions and characters [67-69]. HD is the most common and effective renal

replacement treatment using advanced dialysis machine with removal of waste products and excessive water from blood via delicate dialysis membrane. It is relatively easy for patients to apply because specialized medical personnel can operate the procedure. However, HD patients usually receive dialysis three times a week in the clinic so that their excessive waste product and water generated over 2 or 3 days should be removed only for 4-hours. Erratic changes in volume status, electrolyte and acid base status are developed between dialysis sessions repetitively. This distorted and capricious changes harm cardiovascular system of HD patients, and affect elevated mortality sequentially.

PD uses their own peritoneum, the lining of the abdominal cavity, to filter patient's blood. Dissolved substances such as urea, creatinine, potassium, phosphate and other uremic toxins in the blood are exchanged with indwelled dialysate by mass transfer for 4 to 6 hours and the patient should replace the used dialysate by themselves [70]. PD is preferred to young and active patients due to manageable time and space during dialysis procedures. Fundamentally, it is more physiologic method mimicking natural kidney function of "continuous filtering". Continuous filtration system makes PD patients to be less restricted to their food intake and more beneficial to preserve residual kidney function. Consequently in terms of outcome, PD has shown excellent survival rate compared with HD, especially during the first 2 years after beginning dialysis [71-73] and even after transplantation [74, 75].

Despite these advantages, PD remains as a least-preferred dialysis modality worldwide compared with HD. It is attributed by insufficient removal of uremic toxins, inconvenient and frequent self-exchange system using heavy dialysate bags, infectious complications and metabolic complications such as diabetes, obesity, and metabolic syndrome.

(a)

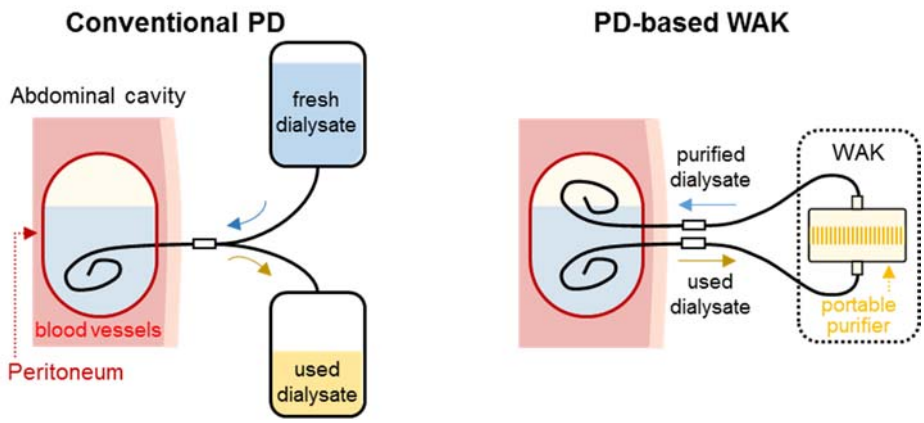

Figure 4.1. (a) Schematic diagram of conventional peritoneal dialysis (PD) and recyclable PD for a portable peritoneal dialysate regeneration system. PD uses patient's own peritoneum, to filter dissolved toxins in a blood with indwelled dialysate for 4 to 6 hours. On the other hand, recyclable PD, which have an integrated portable system of purifying a used dialysate with proper toxin removal rate and refilling the purified dialysate into peritoneum without any self-exchange process, will only provide treatments free from time and space constraints to the patients with end stage renal disease.

(b)

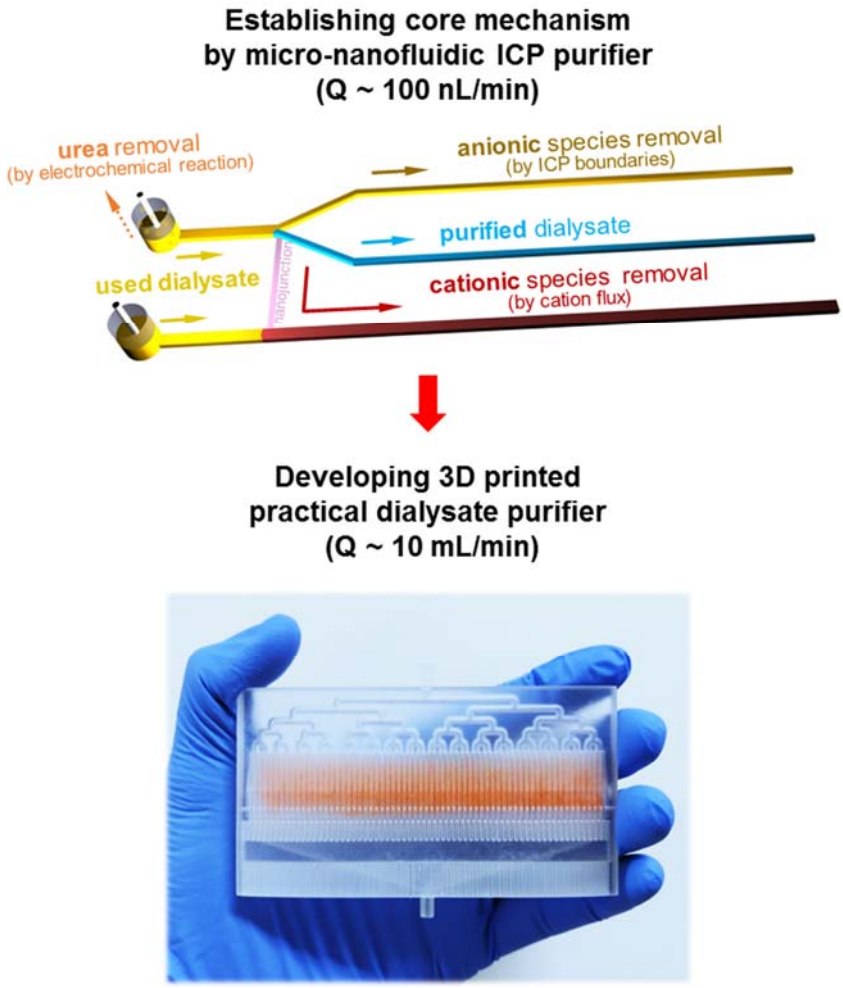

(b) Schematic diagram of body toxins removal mechanism in a micro-nanofluidic platform and a scaled-up device for practical dialysate regeneration. Purified dialysate would be extracted after application of bias between the nanojunction, since urea would be decomposed by non-toxic gases at the anodic electrode, anionic wastes would be rerouted around the ion depletion boundary and cationic species including creatinine would be removed by cationic flux through the nanojunction. This micro-nanofluidic body toxin removal platform would be scaled-up with maintaining a

microfluidic environment for practical utility (~ 10 mL/min) at the clinical point of view.

These inconveniences would be resolved by a portable peritoneal dialysate regeneration system as shown in Figure 4.1 (a). The system offers efficient removal of uremic toxin, simplified self-exchange system, lower infectious and metabolic complications for optimizing PD as an ideal renal replacement modality, maximizing its conceptual merit. It should be capable of automatic withdrawing, purifying the used dialysate and refilling the purified dialysate into peritoneum. Among a number of components, the efficient purification of biological toxic substances would be the key building block. While few mechanisms such as biochemical adsorption or physical filtering has been suggested, inherent limitations such as clogging or frequent replacing the filters, *etc*. hinders further development or commercialization.[76, 77].

In recent years, water treatment society actively seeks a distributed, small-capacity water treatment system of high-energy efficiency, sustainable equipment costs, and minimized environmental problems. Among various proficient candidates, electrochemical techniques such as electrodialysis (ED) [5, 10, 11], electrodeionization (EDI) [8], and capacitive deionization (CDI) [12, 13] fulfills the small-capacity requirements because reverse osmosis (RO) [78] which is the most-popular method would be suitable only for large-scale system. Despite of their unique advantages, none of such technique is capable of purifying wide size-range of target species from salt ions to biomolecular

contaminants simultaneously in a single step process. On the other hand, recently reported ion concentration polarization (ICP) based purification technology [4, 16, 79, 80] properly meets these criteria due to a unique electrical filtration function and high scalability. Briefly, perm-selectivity of nanoporous membrane would initiate a polarization of electrolyte concentration at both sides of membrane and, especially, an ion depletion zone is formed at the anodic side of membrane in the case of cation selective membrane [14, 29]. Since charged species rerouted their path along the concentration distributions near the ion depletion zone, the zone plays a key role to purify wide size-range of contaminants.

In this work, we proposed a nanoelectrokinetic dialysate purification device for continuous flow PD. First of all, a micro-nanofluidic device was employed to verify the mechanism of contaminant removal as the schematic given in Figure 4.1 (b). An *in-situ* visualization and a direct chemical analysis demonstrated that anionic species in a used dialysate rerouted around the ion depletion zone and cationic species including creatinine in a used dialysate was mostly removed by cationic flux through the nanojunction. On the other hand, urea which is known for electrically neutral body toxin was electrochemically decomposed to gas bubbles at the anodic electrode. Therefore, we would continuously obtain a purified dialysate by extracting stream from the ion depletion zone. Finally, this micro-nanofluidic platform was scaled-up using commercial 3D printer. A microfluidic environment was created in this scaling-up device using a confined micro-geometry which

prevented undesirable instability and enhanced the removal of cationic species [24, 34, 35, 81]. *In-vitro* test using a used dialysate obtained from patients who underwent PD and *in-vivo* test on Canine model were conducted for verifying this new scheme.

4.2 Verification of dialysate purification mechanism in micro-nanofluidic platform

Modeled micro-nanofluidic device was shown in Figure 4.2 (a). See experimental method sections for the fabrication process and experimental apparatus. Since a minimum of 100 uL of undiluted sample is required to measure the components in a dialysate solution by Renal Panel, here we maximized throughput by reducing electrokinetic instability with micro-fin structures near the bifurcation point [81], and electrical resistance with double patterned nanojunctions. The used dialysate solutions were continuously injected into both the anodic and cathodic side microchannels at a constant flow rate of 0.4 uL/min. Under these experimental conditions, we successfully generated the ICP phenomenon with developing the ion depletion boundary in front of the nanojunction to separate wastes and purified streams as shown in Figure 4.2 (b). Anionic charged fluorescent dye molecules (Alexa 488, Invitrogen, USA) and carboxylate micro-particles (1 um diameter, Invitrogen, USA) could not pass through the ion depletion boundary and rerouted outside the ion depletion boundary.

(a) (b)

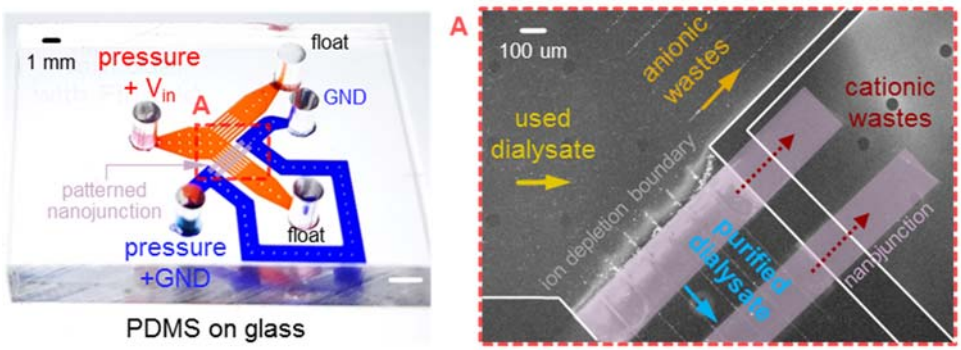

(c)

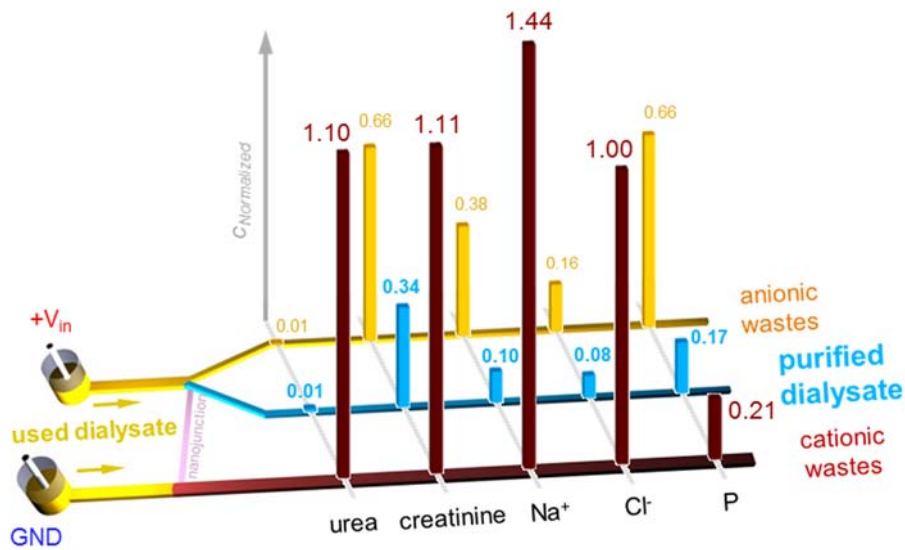

Figure 4.2. (a) A microscope image of fabricated micro nanoelectrokinetic purifier. (b) A microscope image of dialysate purification due to the ion concentration polarization (ICP) phenomenon. (c) A normalized concentration profiles of major indicators at outside (yellow) and inside (blue) the ion depletion boundary of the anodic side streams, and cathodic side (brown) stream.

Each stream was individually extracted and concentration profiles of urea, creatinine, Na^+, Cl^- and phosphorus (P) which are the major indicators to determine status of ESRD patients were quantitatively measured as shown in Figure 4.2 (c). Note that K^+ is also an important indicator, but Na^+ was chosen as a representative indicator because of high measurement accuracy and the same nanoelectrokinetic transportation mechanism applied to both Na^+ and K^+ [82]. The positively charged species (Na^+ and creatinine) were removed from purified stream depending on their electrophoretic mobility [82]. Most of Na^+ ions were transported through the nanojunction by cationic flux and finally, 90 % desalted stream was collected (normalized concentration was 0.1). Creatinine (sub nanometer molecule and one of the major toxin of body wastes from a used dialysate) is electrically neutral at pH 7.4 but a positively charged under pH 7.4. Since dialysate showed slightly acidic property, we confirmed that creatinine follows cation like transportation mechanism under the ICP phenomenon. The concentration of creatinine was decreased at both outside (yellow channel) and inside (blue channel) the ion depletion boundary in the anodic side and increased in the cathodic side (brown channel). Around 50 % of creatinine passed through the nanojunction and around 33 % of it flew through stream of outside the ion depletion boundary. Finally around 17 % of creatinine were left inside the ion depletion boundary so that concentration was significantly decreased in the purified stream (normalized concentration was 0.34). Cl^- was consumed by electrochemical reactions on the anodic electrode to satisfy electro-neutrality in a solution due to the ICP phenomenon

which rearranged concentration profiles near the nanojunction. Remarkably, urea (known as uncharged molecule and one of the major toxin of body waste along with creatinine) was completely eliminated by electrochemical reactions in the anodic side streams including the purified stream (normalized concentrations were 0.01). On the other hand, P was removed from both the anodic and cathodic side channels (normalized concentrations were 0.17). This meant that P could not pass through the nanojunction and was decomposed by electric field across the channels.

4.3 Design and fabrication of the device

While the feasibility of nanoelectrokinetic purifier for a continuous dialysate purification was demonstrated in a micro-nanofluidic platform, the throughput of the device is insufficient for practical dialysate recycling for either human or animal test. In this chapter, 3D printed macroscale exquisite device was fabricated for the throughput enhancement. The basic idea of this macro device is creating a microfluidic environment in a macro-fluidic device [83]. While the expansion of ICP layer is obviously requisite to filter dialysate at this high throughput device, ICP device loses function if the channel dimension becomes larger than $O(100)$ um as similar as other micro-nanofluidic devices [81, 84]. The important characteristics (or regimes) of ICP formation in micro-nanofluidic platform were reported [35] as (1) surface conduction (SC), (2) electroosmotic flow (EOF) and (3) electroosmotic instability (EOI). These plays a critical role of ion transportation through the nanojunction as well. As the characteristic length of channel changes, SC and EOF and EOI dominates over the ion transportation at very thin channel (< 5 um) and at thin channel (< ~$O(100)$ um) and at wide channel (> ~$O(100)$ um), respectively, so that this macroscale device should have the EOI characteristics. However, the EOI dominant system always has an avoidable instability [85-87] and high-energy consumption as a result of lowering overlimiting conductance [51]. In order to adjust the regime from EOI to EOF or SC, micro fin structures were previous employed in 2-dimensional micro-nanofluidic device [81]. The fins were able to suppress the EOI and we could

integrate and enhance the throughput up to dozens of conventional ICP devices of Q= ~5 uL/min. However, channel widening in a single plane (*i.e.* 2-demensional expansion) is unable to provide more than lab scale throughput. Thus, expansion of the fins at z-direction (*i.e.* 3-dimensional) contrived a mesh structure that plays the identical role of the fins.

	Driving mechanism	Junction type	Electrode contact to dialysate	Schematic	Applied potential	Average removal ratio (%)				
						urea	creatinine	Na	Cl	P
#1-1	Electro-chemical reaction	x	internal		low (< +1.7 V vs SCE)	8.10	5.32	8.40	8.91	4.55
					high (> +1.7 V vs SCE)	96.76	4.52	14.50	31.19	52.27
#1-2	Electro-chemical reaction	micro	internal		low	9.35	-6.75	-4.30	-2.02	5.00
					high	99.55	2.49	1.65	1.09	2.27
#2-1	ICP	nano	internal		low	-3.60	23.82	58.68	67.39	81.82
					high	98.88	66.23	89.52	92.38	82.76
#2-2	ICP	nano	internal		low	-0.62	0.43	11.76	16.30	-7.89
					high	85.48	71.69	51.26	82.61	52.63
#2-3	ICP	nano	external		low	-1.56	0.18	62.31	46.97	85.42
					high	-6.31	32.13	70.66	77.72	93.18

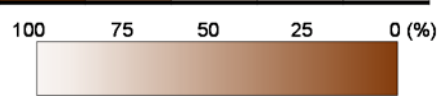

Table 4.1. The table of control experiment result for verifying dialysate purification mechanism.

Dialysate purification mechanism by ion concentration polarization (ICP)

Control experiments were performed with various types of junction and location of electrode to confirm dialysate purification conditions including

urea and Phosphorus (P) removal mechanism as shown in table 4.1. Outward stream was collected from outlet reservoir of each case, and average removal ratio of urea, creatinine, Na+, Cl- and P were quantitatively measured by Renal Panel.

Firstly, electrochemical reaction condition was demonstrated without using nanojunction in a microfluidic device (#1-1 in the table 4.1). Two Electrodes were placed inside a single microchannel, one for inlet reservoir and the other for outlet reservoir, without using any junctions. A used dialysate was filled in microchannel, and both positive voltage and pressure were applied in inlet reservoir. In this case, all species were removed within 10 % at low electrical potentials. However, urea was completely eliminated, Cl- was ~30 % and P was ~50 % removed at high electrical potentials. We obtained similar results when microjunction was built between an anodic side bifurcated microchannel and a cathodic side microchannel instead of building nanojunction (#1-2 in the Table 4.1). In this case, only urea was completely eliminated and other species were remained including P. Here minus removal ratio is measured due to evaporation at the reservoirs. The reason why urea was completely removed is because of the electrochemical reaction. It was reported that urea was decomposed to nitrogen and carbon dioxide gas at high potentials (over 1.7 V versus saturated calomel electrode (SCE)) by direct oxidation process at the electrode surface as following equations [88-90]. Eq. (1) refers the anodic reaction, eq. (2) refers the cathodic reaction, and eq. (3) refers the overall reaction.

$$CO(NH_2) + 6OH^- \rightarrow N_2 + 5H_2O + CO_2 + 6e^- \quad (1)$$

$$6H_2O + 6e^- \rightarrow 3H_2 + 6OH^- \quad (2)$$

$$CO(NH_2) + H_2O \rightarrow N_2 + 3H_2O + CO_2 \quad (3)$$

Here, nitrogen and carbon dioxide gas product from this electrochemical decomposition are harmless to the human body. Note that urea decomposed to nitrogen oxidants which is harmful to human body at lower potentials (below 1.6 V versus SCE) or natural oxidation condition.

Secondly, the ICP condition was implemented with applying nanojunction in a microfluidic devices. As we mentioned above paragraph and section 2 in paper, urea was completely eliminated at high potentials and other species were removed by electrical transportation due to the ICP phenomenon (#2-1 in the Table 4.1). Applying a low potential reduced the removal rate of all components. Similar results were obtained when two outlet reservoirs were combined into one outlet reservoir (#2-2 in the Table 4.1). In this case, overall removal ratio was lower than #2-1 in the Table 4.1, but creatinine removal ratio was almost the same. To separate the ICP phenomenon and electrochemical reaction, we built 3 independent microchannels, one for an anodic at the top side, another for a sample flowing at the middle side and the other for a cathodic at the bottom side (#2-3 in the Table 4.1). This structure is similar to that of an electrodialysis (ED) cell. In this case, the ICP phenomenon was still successfully developed at the middle bifurcated

channel since electric field across the nanojunction from the top anodic side channel to the bottom cathodic side channel generated strong cationic flux. Note that urea was remained without any change, but creatinine and Na^+ were removed by electrical transportation due to the ICP phenomenon. On the other hand, in section 2, we discussed that P was removed by the electric field because P was removed from both the anodic and cathodic side channels. Here, we found additional evidence that P removal ratio was always higher in the ICP conditions (#2-1, #2-2 and #2-3 in the Table 4.1) than in electrochemical reaction conditions (#1-1, #1-2 in the Table 4.1). It meant that the P removal ratio was related to the electric field strength since electric field is highly amplified inside the ion depletion zone [33, 49].

From these analysis results, we can conclude that dialysate purification can only be successfully achieved when the ICP phenomenon (the case of #2-1 and #2-2) is generated by the electrode inside the injected dialysate stream.

4.3.1 Development of high-throughput nanoelectrokinetic device

ICP separator using planar mesh structure without buffer

Planar type mesh structure was developed as a first prototype to substitute surface patterned Nafion of microchannel based ICP separator. The key structure of the device is comb-shaped stabilizer which suppresses undesirable instability of ICP phenomenon, acting like 3-dimensional fin. Different from previous ICP separators, brine channel is used as buffer channel where enrichment zone forms. The elimination of buffer channel leads to low complexity of the system. As per demonstrations, a single device can process a sample at 200 uL/min and one can increase the throughput by connecting several unit as much as one desire.

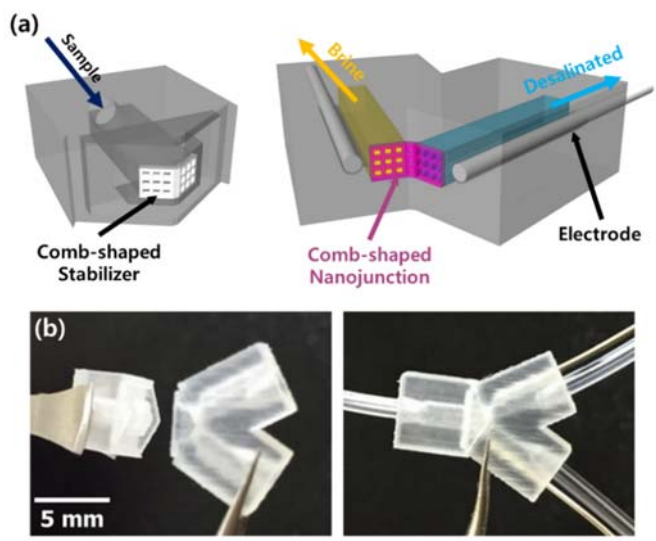

Figure 4.3. (a) Schematic image of two units of macro ICP separator. (b) 3-D printed units and their assembled image.

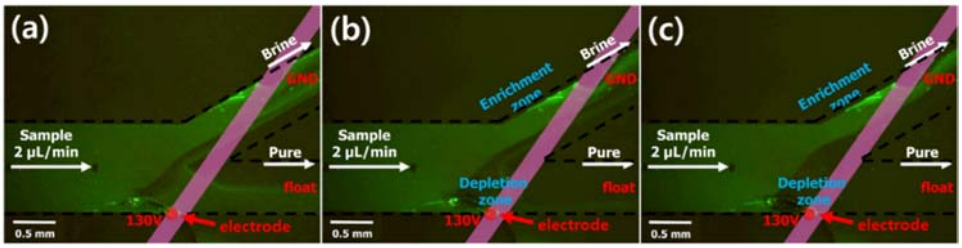

Figure 4.4. The operation image of brine-enrichment zone combined microfluidic ICP separator, at t = (a) 1 s, (b) 11 s and (c) 21 s.

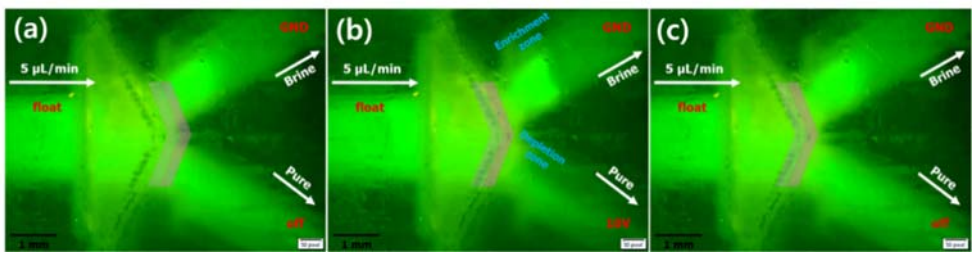

Figure 4.5. Operation image of 3-D printed macro ICP separator, after voltage applied (a) 1s / (b) 180s. (c) 30s after voltage off.

First, we build framework of the device by ProJet 3510 SD and use VisiJet as a material. The material is partly transparent and also has florescence. Because of these characteristics, it is hard to observe or capture fluorescent image of device operation. The device is printed out two separated units as figure 4.4, to coat Nafion on the purple-colored mesh. Nafion is manually coated on the mesh. Comb-shaped stabilizer and Nafion coated mesh both has 200um x 200um square holes and 50um thickness as well. Next, assemble two parts, so that the stabilizer and the mesh are contacted. Finally, insert Ag electrodes to side holes of both brine and purification channel. To demonstrate this macro ICP separator, 1mM NaCl + Alexa 488 dye solution is used.

Preliminary test with 2-D model was conducted to confirm feasibility of brine-buffer merged ICP separator. Operation strategy of the 3-D model is exactly the same as 2-D brine-enrichment zone separator (figure 4.5). Voltage is applied on the edge of purification channel (shown as red circle) and ground on the end of brine channel. While it takes longer to fully develop to separation mode compared with the buffer-grounded ICP separators, the schemes successfully separate the sample shown in figure 4.5

After 2-D model test, 3-D model was tested. As the same role as surface-patterned Nafion in 2-D separator, Nafion coated mesh is transportation path of cations from purification channel to brine channel. The other part, comb stabilizer suppresses vortices inside the ion depletion zone. Thus it contacts on Nafion coated mesh to restrict growth of vortices. The size of the prototypes are designed to have 1mm x 1mm and 2mm x 2mm square cross-sectional area, respectively and the demonstration with the former is shown in figure 4.6. Flow rate and voltage are applied range from 5 to 50 uL/min and 10 to 50 V, respectively.

(a) (b)

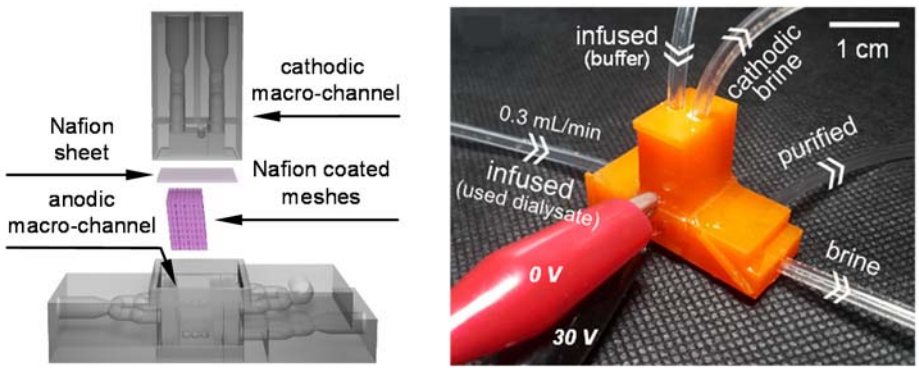

Figure 4.7. (a) Exploded view of 3D printing blocks for a macro-fluidic device. To assemble a macro-fluidic device, nanoporous Nafion sheet and Nafion coated mesh blocks were inserted between anodic and cathodic macro-blocks. (b) Assembled macro-fluidic device. 0.3 mL/min and 30 V external sources were applied to the device and the purified, the brine and the cathodic brine streams were collected and analyzed.

(a) (b)

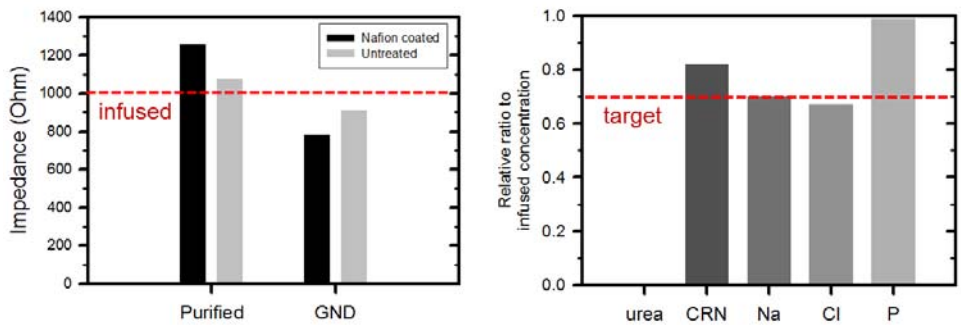

Figure 4.8. Removal efficiency of the macro ICP purifier. The results satisfied the operation criteria of the continuous dialysate recycler (~30% removal) with completely removed urea.

Prototype of dialysate recycler including buffer

The expansion of ICP layer is requisite to filter dialysate at macrofluidic system. However, prototype without buffer could handle only a low concentration. Thus, we contrive another system which has Nafion coated mesh and buffer including Nafion sheet depicted in figure 4.7 (a). The frame of the mesh is made of 3D-printed photopolymer (BV-012, MiiCraft) and coated by Nafion. It performs as the transportation pathway of cations to arise ICP, which carries out the similar role of surface-patterned Nafion at micro/nanofluidic system. The mesh was designed to maximize contacting area with dialysate flux, for high cation transportation rate. Divided by Nafion sheet, cations migrates from anodic macro-channel to cathodic macro-channel without flow interference. Cations are depleted at the vicinity of Nafion sheet after applying electric field from anodic to cathodic channel. The mesh performs as the medium to expand ion depletion layer, which enable to occur only thin (<100um) depletion layer if there were no mesh structure. Anodic electrode is located on brine channel and cathodic electrode is located on buffer channel. The products from electrode reaction go to each brine/buffer channel so that do not affect purified dialysate. The actual device operates as figure 4.7 (b) after fabrication and assembly.

The performance of the device depends on voltage and flow rate. Purification ratio enhances as higher voltage at the same flow rate, because more cation transported through Nafion coated mesh. In addition, the products from electrode reaction could bring imbalance of pressure

distribution, so that we also consider it to decide voltage and flow rate. To begin with comparison test with Nafion coated/untreated mesh installed device was conducted. The performance of purifier with Nafion coated mesh was 4 times better than untreated one as figure 4.8 (a). After comparison test, CRN was removed ~20% and urea was removed over 90% at the 0.3 mL/min of used dialysate infusion and 30 V condition (figure 4.8 (b)). Target removal ratio is hard to satisfy the target by adjusting operating condition, so the design of purifier needs to be upgraded.

4.3.2 Conclusive design of the device for dialysate recycle

In the clinical point of view for continuous flow dialysate purification, the clearance of various uremic components is unnecessary to over 99 % which is strongly required level for potable water. This is because one has to preserve the essential proteins that can be significantly lost by PD, while it is necessary to remove excessive body ions and toxins such as urea and creatinine. When performing continuous flow PD, we initially aim to remove 30 % of the body toxins at a flow rate of 10 mL/min for the canine model, since sudden removal of ions and toxins may cause cerebral edema by disequilibrium syndrome [91] and/or brain edema and fatal arrhythmia by acute hyponatremia or hypokalemia [92]. These target values could be adjusted depending on the patient's health and physical conditions. Moreover, volume loss due to the dialysate flowing through the anionic species removal channel which contained a small amount of creatinine and a large amount of such protein rejected by the ion depletion boundary should be eliminated. As refer to the micro-nanofluidic dialysate purification results shown in figure 4.2 (c) and Table 4.1, we set a strategy to design a single channel in the anodic side by combining outside and inside the ion depletion boundary channels (#2-2 in the Table 4.1). Such design enables one to prevent unwanted fluid loss and achieve enough removal ratio of toxins over than 30 %.

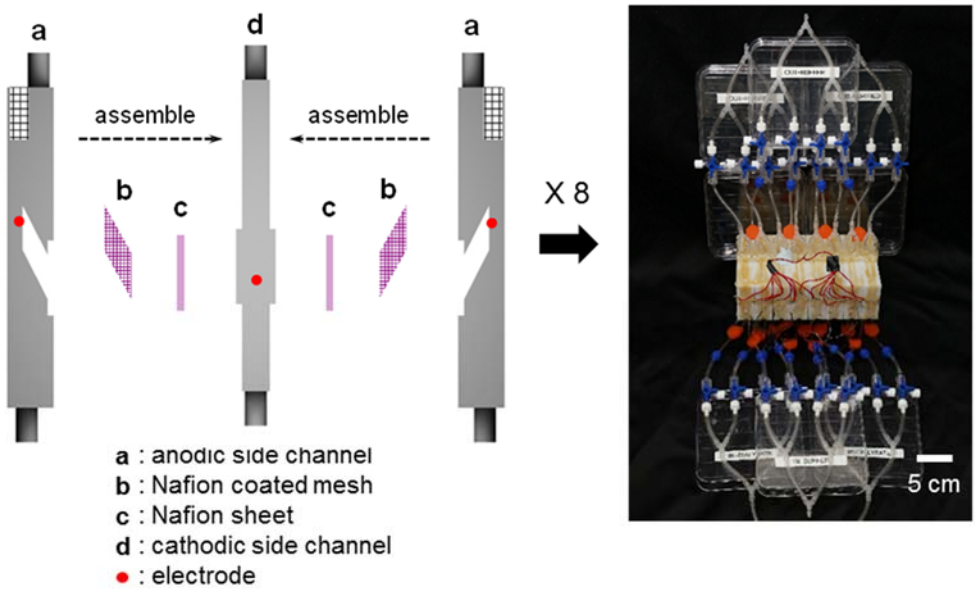

Figure 4.9. Exploded view of a single module of the macro nanoelectrokinetic purifier and a real image of assembled multi module device in parallel. A single module of macro nanoelectrokinetic purifier is composed of anodic side channel, Nafion-coated mesh, Nafion sheet and cathodic channel. Eight modules can be connected in parallel to achieve nanoelectrokinetic purification throughput of 10 mL/min.

Based on aforementioned concept of nanoelectrokinetics and clinical point of view for continuous flow dialysate purification, we developed the macro nanoelectrokinetic purifier which is composed of an anodic side channel, Nafion-coated mesh, Nafion sheet and a cathodic side channel as shown in figure 4.9. The device was designed to have similar operating principle of micro nanoelectrokinetic purifier and able to be assembled in parallel. Here

the cathodic side channel was designed to share two anodic side channels for increasing integration efficiency.

(a) (b)

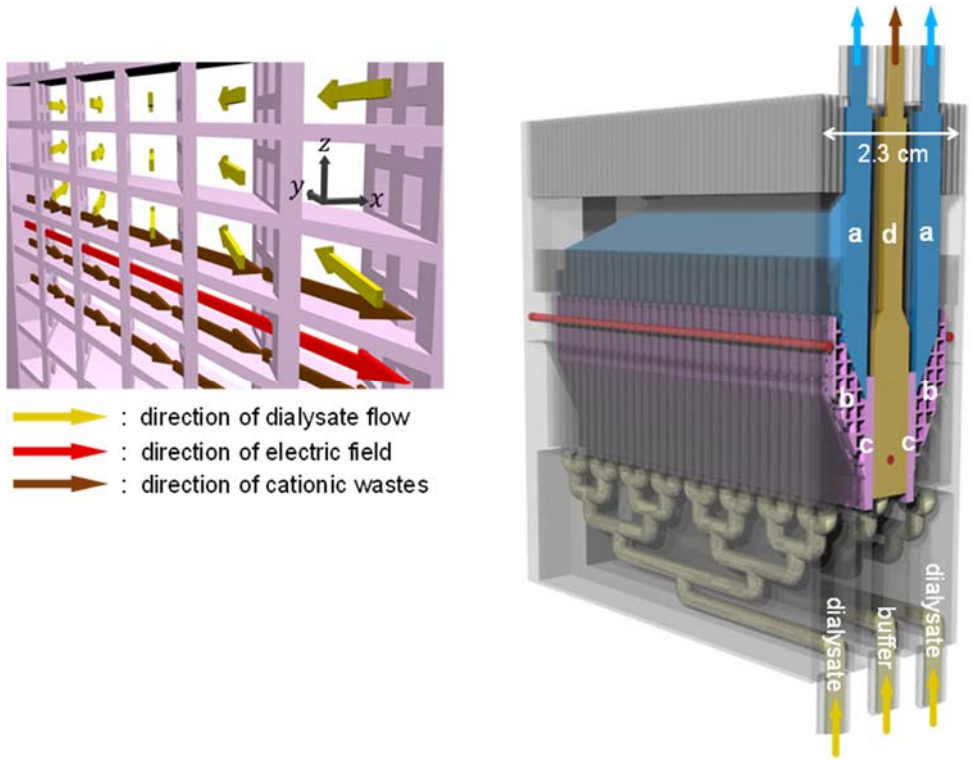

Figure 4.10. (a) Schematic diagram of Nafion coated mesh design approach. Coated Nafion on the mesh surface ensures that the cationic wastes are transported towards the Nafion sheet along the direction of the electric field so that purified dialysate passed through the mesh perpendicular to the electric field. (b) Cross sectional view of an assembled single module of the macro nanoelectrokinetic purifier. The macro nanoelectrokinetic purifier is 10 cm wide, 2.3 cm high, 5.5 cm high and consists of a stack of 64 micro-nanofluidic devices.

Nafion sheet was adopted to separate the anodic and cathodic side channels, which not only prevents fluidic interference but also passes the positively charged species. Nafion-coated mesh was installed to enable sufficient and stable purification in a wide macro-fluidic channel. The specificity of Nafion-coated mesh design approach was shown in figure 4.10 (a). Mesh structure which had micro-scale width, length and height was installed to form micro-nanofluidic regime in macro-fluidic channel. Coated Nafion on the mesh surface ensures that the positively charged species are transported towards the Nafion sheet along a direction of electric field. Therefore, cationic wastes in a used dialysate were removed through Nafion-coated mesh and Nafion sheet along with an applied electric field direction, and a purified dialysate passed through the mesh perpendicular to the electric field direction. Cross sectional view of assembled parts was shown in figure 4.10 (b). In principle, 64 layer of micro-nanofluidic devices were stacked in this single macro nanoelectrokinetic purifier module. The single unit module of 5.5 cm height, 10 cm length and 2.3 cm width was manufactured after optimization, which could purify a used dialysate at the throughput of 1.33 mL/min. Finally, a multiple module device with a processing capacity over 10 mL/min was completed by connecting eight single modules in parallel, which throughput was 100,000 times enhanced compared with micro-nanofluidic device.

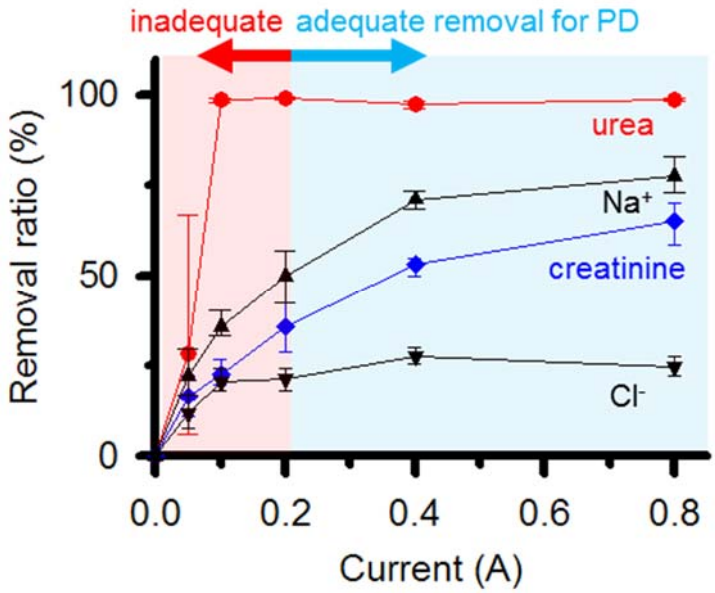

Figure 4.11. Graph of toxins removal performance of a single module of the macro nanoelectrokinetic purifier at the throughput of 1.33 mL/min.

The performance test for a single unit of the dialysate purifier was demonstrated as shown in Figure 4.11. A used dialysate and a fresh dialysate were infused 1.33 mL/min to the anodic and cathodic side channels, respectively. The current source was applied from 0.05 to 0.8 A and the steady-state voltage was measured simultaneously from 5.8 to 25.3 V. At each condition, single-path purified sample was measured every 20 minutes and processed 60 minutes totally. Urea was started to be decomposed completely from above 0.1 A and creatinine was removed over 30 % at more than 0.2 A. The removal performance of the macro nanoelectrokinetic purifier was directly related to an applied electrical current, but the removal ratio showed a tendency to saturate at 0.4 A or higher. From these results, we set an electric

application strategy (0.2 A to a single module of throughput 1.33 mL/min, 1.6 A to eight multi modules of 10 mL/min) to achieve more than 30 % removal of body toxins for following in-vitro and in-vivo experiments.

4.4 Experimental methods

4.4.1 Fabrication of micro nanoelectrokinetic purifier

Micro-nanofluidic device, consisted of a bifurcated anodic side microchannel, nanojunction, and a single cathodic side microchannel, was fabricated using Polydimethyl siloxane (PDMS, Sylgard 184 Silicone elastomer kit, Dow Corning) substrate and Nafion polymeric solution (20 w.t.% resin, Sigma Aldrich). Firstly, to build fluidic channels, both the anodic and cathodic side microchannels were designed to have the dimension of 1 mm width and 15 um depth. A pre-polymer of PDMS and curing agent were mixed with 10:1 ratio and bubbles were bled in a vacuum chamber about an hour. Pouring the mixed polymer solution onto the microchannels patterned master and curing it in an oven about 4 hours. Secondly, to build nanojunction, Nafion solution was utilized as a cationic perm-selective nanoporous material and patterned between bifurcated point of the anodic side microchannel and the cathodic side microchannel using surface patterning method [51, 93, 94]. Finally, the PDMS block having fluidic channels and the slide glass having the solid Nafion nanojunction were accurately aligned and chemically bonded by using a plasma bonder (Cute-MP, Femto Science, Korea). The assembled device was shown in Figure 4.9.

4.4.2 Apparatus for micro-nanofluidic experiment

Both external voltage sources and pressure sources were required to initiate asymmetric ion depletion boundary generation. An external voltage was applied across the nanojunction using a source measurement unit (SMU 238, Keithley, USA). The analyte and buffer solutions were injected into the microchannel using a syringe pump (PHD 2000, Harvard apparatus, USA). An inverted fluorescence microscope (IX-51, Olympus, Japan) and a CCD camera (DP73, Olympus, Japan) were used to detect and image the electrokinetic flow in the microchannel. Commercial software (CellSense, Olympus, Japan) was used to synchronize the CCD camera with the microscope and to analyze the images. The components in a dialysate was analyzed by renal function panel (7180 HITACHI Automatic Analyzer, Japan).

4.4.3 Apparatus for macro-fluidic experiment

A commercial 3D drawing program (RhinoCeros 5.0) was used to design the practical electrokinetic dialysate purifier. The purifier is composed of anodic compartments, mesh structure, Nafion sheet (0.002 inch thickness, Sigma Aldrich) and cathodic compartments as shown in Figure 4.9. The frames of these channels were printed by Projet 2500+ (3Dsystems, USA) with MJP RWT resin (3Dsystems, USA). The frame of the mesh structure was 3D printed by M125 (MiiCraft, USA) with photopolymer FC-2 (MiiCraft, USA). 8 of unit macro devices were assembled for the final device which had the throughput of 10 mL/min. Epoxy adhesive was glued to bond each unit device. Tigon tubes (i.d. 3.2 mm, ISMATEC) were used to connect to the in-vitro circuit. An external voltage was applied using a source measurement unit (Lambda zup 36-6, TDK). The analyte and buffer solutions (used dialysate from Seoul National University Hospital) were continuously injected with a constant flow rate into both the anodic and cathodic side channels using a peristaltic pump (custom manufactured from Seoul National University, Department of Biomedical Engineering, College of Medicine and Institute of Medical and Biological Engineering, Medical Research Center). Each stream was extracted individually and concentration profiles of Na^+, Cl^-, creatinine, and urea were quantitatively measured by Renal Panel (7180 HITACHI Automatic Analyzer, Japan).

4.4.4 In-vivo canine model using chronic renal failure beagle dogs

Adult male Beagle dogs (age 14–16 months; weight 8–11 kg) were used for 15/16 nephrectomy chronic kidney disease model. For inducing partial infarction of left kidney, seven of eight left renal arteries were ligated. One week later, contralateral kidney was removed creating 1/16 remnant kidney. Sixteen weeks after second operation, 60 percent beagles showed sustained high serum creatinine (Scr>2.0 mg/dl) and proteinuria (Protein to creatinine ratio >1.5 g/gCr) levels, namely proper modeling of chronic kidney disease. Among established model, two dogs were performed peritoneal catheter insertion operation. In supine position, the anterior abdominal wall was incised bilaterally and the peritoneal membrane was exposed. Two Double-cuff Tenckhoff catheters were inserted into abdominal cavity through each incision site bilaterally and purse string suture was performed to avoid dialysate leakage.

For the beginning, 600 mL (60 cc/kg) of a fresh dialysate was filled into the abdominal cavity of the beagle dog. Then, the exchange of the substances between the dialysate in the abdominal cavity and the serum occurs actively through the peritoneum so that body toxins in the serum was newly diffused into the abdominal cavity. After 4 hours, the contaminated dialysate in the abdominal cavity was withdrawn outside by the peristaltic pump and passed through a filter firstly and the macro nanoelectrokinetic purifier secondly to be purified. Note that we utilized silk-fibroin48 with Renamezin coated filter since silk-fibroin pores filtrate in-vivo debris which was flew out of the

abdominal cavity of the dog and Renamezin adsorbed creatinine. Then purified dialysate was injected into the abdominal cavity again after passing the sensor part for monitoring the concentration of urea and electrolyte. The buffer unit corresponding to the cathodic side is implemented so as to have an independent circuit to be circulated by an additional used dialysate. Therefore, the continuous flow PD process was automated by reinjecting the purified dialysate into the abdominal cavity. Note that we set 3 sampling points, one for serum of the dog, second for exit of the abdominal cavity of the dog and third for exit of the nanoelectrokinetic purifier.

For a long-term in-vivo experiment, several treatments were applied as shown in figure 4.11. An adult female beagle (age 5 years; weight 11kg) was used for total nephrectomy model. Unlike 15/16 nephrectomy chronic kidney disease model, bilateral kidneys were removed simultaneously, meaning immediate loss of whole kidney function. After operation, dialysis was halted for 24 hours in order to take time to accumulate uremic toxins. First conventional PD was performed with 40 cc/kg every 2 hours for 3 days continuously. We used 1.5 % or 2.5 % dextrose dialysate solution, aiming for a zero fluid balance. After another two days' halt of dialysis, we secondly performed conventional PD with escalated dialysis dose of 60 cc/kg. For daytime, we exchanged a total of 4 times of peritoneal dialysate fluid every 2 hours with 1.5 % or 2.5 % dextrose solution. For nighttime, 7.5 % icodextrin solution was indwelled for 16 hours. In this way, 5 days of dialysis treatment was performed. Subsequently, 24-hour long-term in-vivo experiment was

conducted. Additional control panel was adopted to stop the purifier at emergency. Here only macro nanoelectrokinetic purifier (10 mL/min throughput) was utilized as a dialysate purification block for continuous flow PD. The filter was not applicable for long-term utility since debris in a peritoneal fluid blocked the filter pores in short time (less than 3 hours). Dialysate purification process was carried out continuously and the concentration changes of the toxins and electrolyte were measured by sampling every 20 minutes.

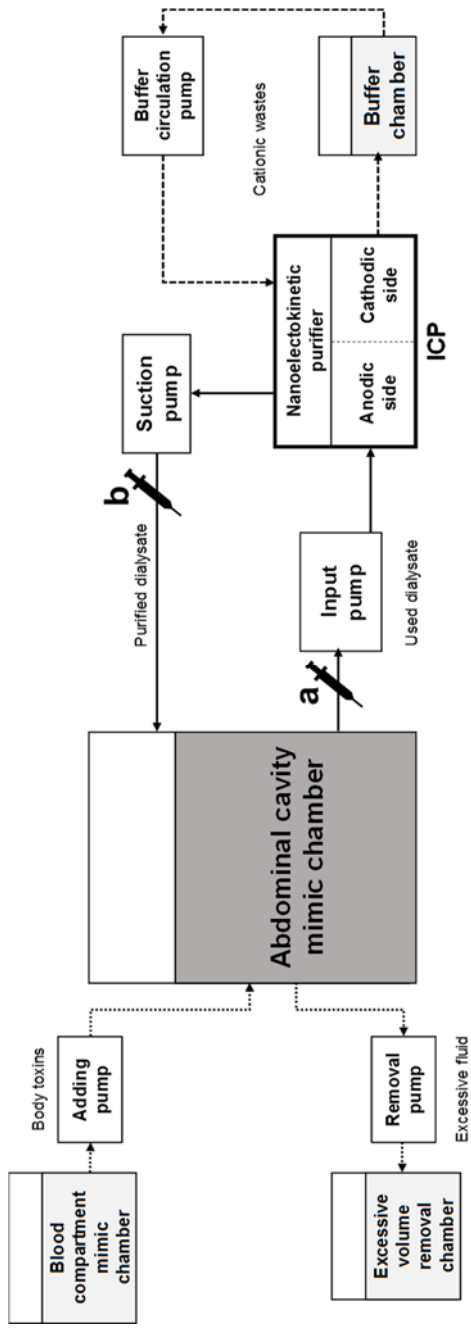

Figure 4.12. A block diagram of in-vitro experiment. A used dialysate which was initially in the abdominal cavity mimic chamber flew into the anodic side of the macro nanoelectrokinetic purifier and the extracted purified dialysate was injected again into the abdominal cavity mimic chamber.

4.5 Experimental results

4.5.1 *In-vitro* closed-loop circulation of peritoneal dialysate using the device

In-vitro closed-loop experiment was conducted to simulate the performance of continuous peritoneal dialysate purification for continuous flow PD, by the complete circuit shown at figure 4.12 (a). The images of in-vitro experiment were shown in figure 4.13. Here we used a macro nanoelectrokinetic purifier (10 mL/min throughput) with eight single modules connected in parallel. The 1-1.6 A of electrical current was applied to pass between electrodes. In the beginning, 2 L of a used dialysate was filled in the abdominal cavity mimic chamber which simulated a peritoneal fluid volume in the abdominal cavity of the body. We additionally set blood compartment mimic chamber and excessive volume removal chamber to mimic the uremic toxin transport into the abdominal cavity from blood compartment through the peritoneum. A used dialysate in the blood compartment mimic chamber was flew into the abdominal cavity mimic chamber (2 mL/min) and an excessive volume of dialysate flew from the abdominal cavity mimic chamber into the excessive volume removal chamber (2 mL/min). The total volume level was thus maintained in the abdominal cavity mimic chamber. In the meantime, the used dialysate in the abdominal cavity mimic chamber was flew into an anodic side of the macro nanoelectrokinetic purifier (10 mL/min), and then a purified dialysate was extracted from the device. Finally, the purified dialysate was from it. Then, the purified dialysate was reinjected into the abdominal cavity

mimic chamber. This dialysate circulation process was continuously repeated to purify the used dialysate in the abdominal cavity mimic chamber. On the other hand, the buffer unit corresponding to a cathodic side of the macro nanoelectrokinetic purifier had an independent circuit. The chamber was initially filled in a fresh dialysate and the dialysate was continuously circulated (10 mL/min). The samples at “a” and “b” were measured every 20 minutes for 2 hours and every 2 hours for the next 10 hours.

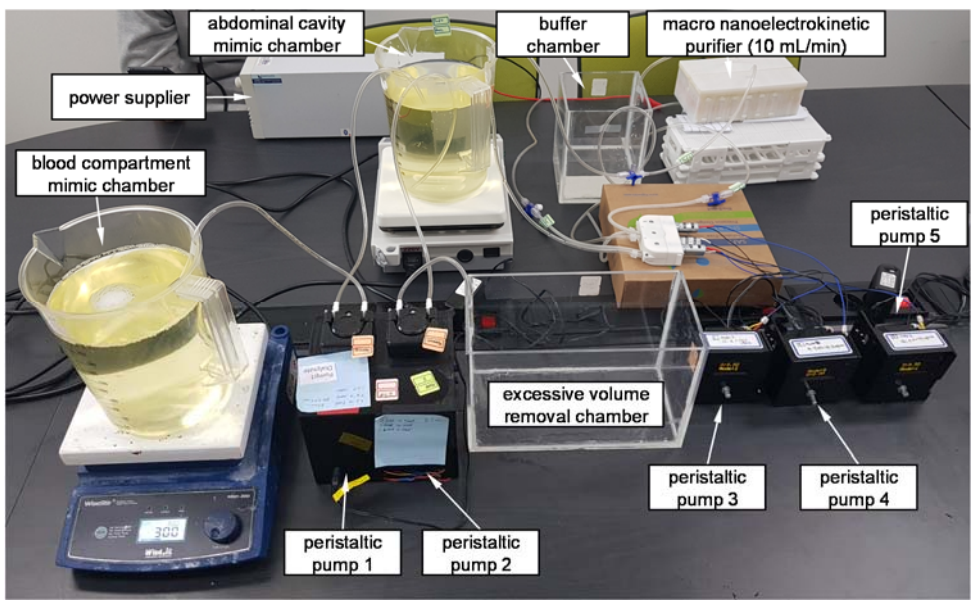

Figure 4.13. An image of in-vitro closed-loop experiment set-up for simulating the circulation of dialysate in the abdominal cavity.

A closed-loop experiment for simulating the circulation of dialysate in the abdominal cavity was set up as shown in figure 4.13. The 2 L of a prepared used dialysate was filled into the abdominal cavity mimic chamber. A used

dialysate in a blood compartment mimic chamber was flew into the abdominal cavity mimic chamber at a flow rate of 2 mL/min by a peristaltic pump 1, and an excessive volume of dialysate flew from the abdominal cavity mimic chamber into the excessive volume removal chamber at the same flow rate by a peristaltic pump 2. In the meantime, the used dialysate in the abdominal cavity mimic chamber was passed through the macro nanoelectrokinetic purifier at a flow rate of 10 mL/min by a peristaltic pump 3. Purified dialysate was withdrawn from the macro nanoelectrokinetic purifier by a peristaltic pump 4, which is used for stable maintenance of the flow rate, and discharged again into the abdominal cavity mimic chamber. The cathodic buffer channel is implemented so as to have an independent circuit to be circulated at a flow rate of 10 mL/min by a peristaltic pump 5.

The single-path removal ratio of body toxins (urea, creatinine) and electrolyte (Na^+, Cl^- and P) during 12 hours was shown in the following figure 4.14 (a). The removal ratio of samples after single-path purification was calculated as (1-(concentration at node b)/(concentration at node a)) 100 (%). Urea was totally eliminated during initial 4 hours of operation. The average removal ratio of creatinine was measured at 27.8 % level which is proper value of clinical point. As similar as creatinine, the average removal ratio of Na^+ was measured at 34.5 % level and Cl^- was measured at 9.4 % level, respectively.

(a)

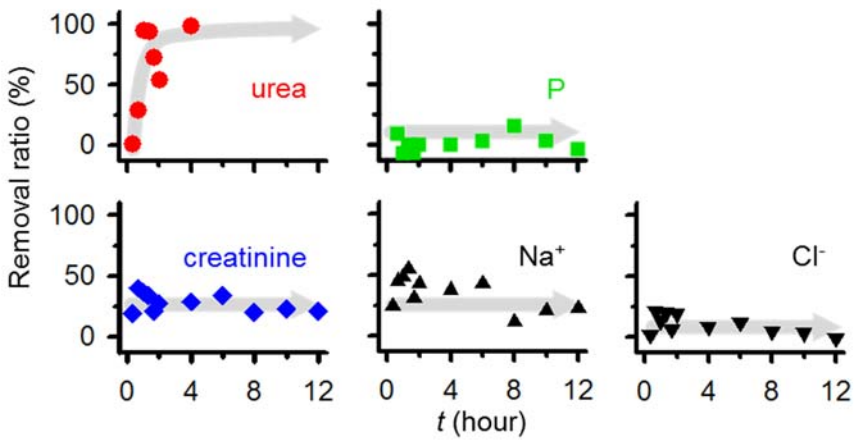

(b)

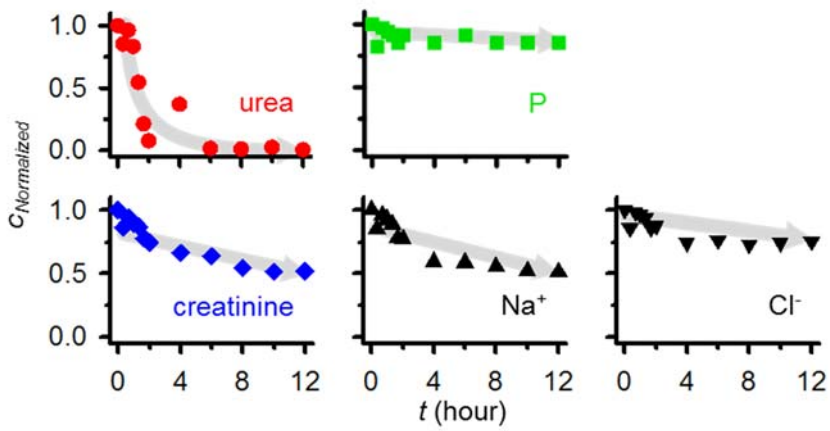

Figure 4.14. (a) Graphs of the removal ratio of the major indicators by the macro nanoelectrokinetic purifier with respect to time. Urea was totally eliminated during initial 4 hours of operation and other species had a constant removal tendency. (b) Graphs of the normalized concentration of the major indicators in the abdominal cavity mimic chamber with respect to time. The concentration of urea was steeply decreased during initial 2 hours and other species showed a linear decreasing tendency.

Next, the concentration change of the used dialysate in the abdominal cavity mimic chamber was measured as shown in figure 4.14 (b). The concentration of urea was steeply decreased during initial 2 hours and finally reached at 0.004 % compared to its initial concentration because the entire used dialysate (~2 L) had passed through the macro nanoelectrokinetic purifier with removal ratio over than 90 %. On the other hand, the concentration of creatinine, Na^+, Cl^- and P were linearly decreased and finally they reached at 51.9 %, 51.6 %, 75.0 % and 85.3 % compared to their initial concentration, respectively. This *in-vitro* experiments were repeated more than 10 times for guaranteeing a reproducibility and the removal rate and normalized concentration in figure 4.14 (a) and (b) were chosen from one of the experiments. Therefore, we concluded that the rate of body toxins removal by macro nanoelectrokinetic purifier satisfied the clinical criteria.

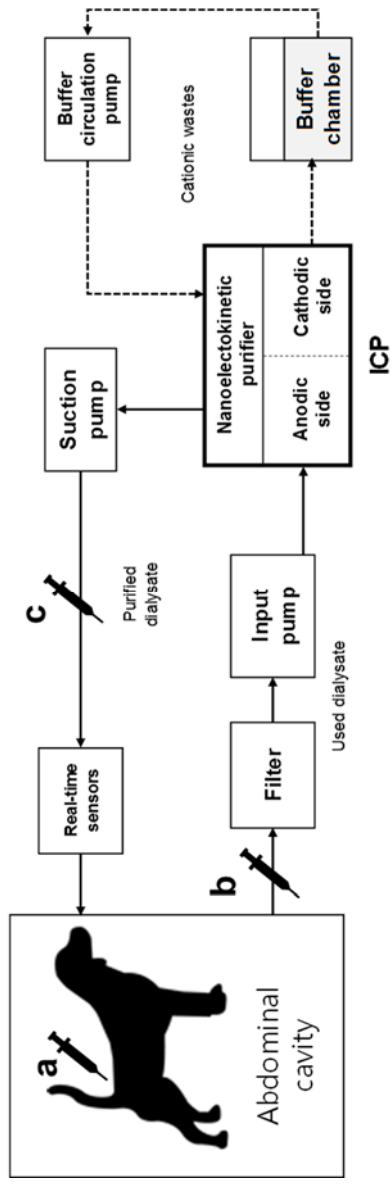

Figure 4.15. A block diagram of in-vivo experiment with a model of chronic renal failure beagle dog. A used dialysate in the abdominal cavity of the dog was withdrawn at 10 mL/min. The cathodic side of the macro nanoelectrokinetic purifier was initially filled with a fresh dialysate and circulated at 10 mL/min independently with the cationic wastes being continuously injected from the anodic side.

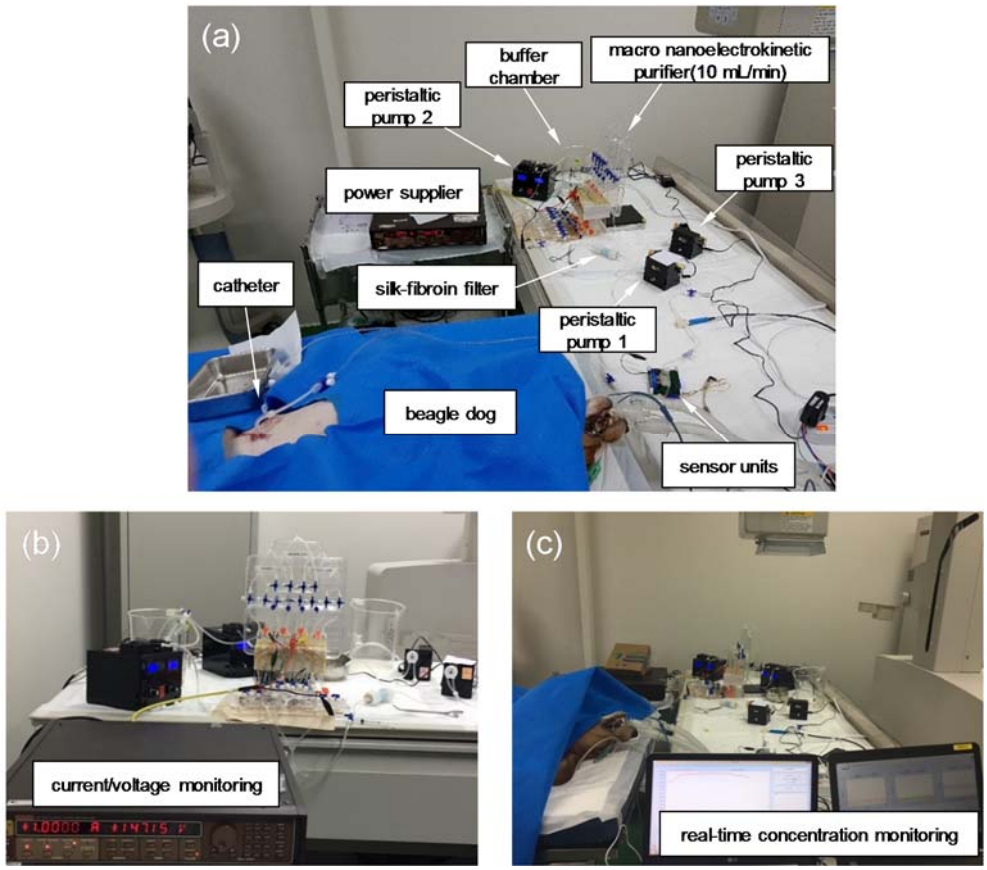

Figure 4.16. (a) An image of in-vivo closed-loop experiment set-up for the circulation of dialysate in the abdominal cavity of the beagle dog, (b) power supply and current/voltage monitoring system and (c) real-time concentration monitoring system.

4.5.2 *In-vivo* closed-loop circulation of peritoneal dialysate using the device with canine

The preparation of the *in-vivo* experiment was determined based on the removal rates of toxins and other substances identified in the *in-vitro* test results. The block diagram of *in-vivo* experiment was depicted as shown in Figure 4.15 and the sampling nodes were also indicated. To implement a real peritoneal dialysis environment, (1) a model of chronic renal failure beagle dog was prepared and (2) a catheter was inserted at the entrance of the abdominal cavity of the dog (from Seoul National University Hospital). The 1 A of electrical current was applied to pass between electrodes.

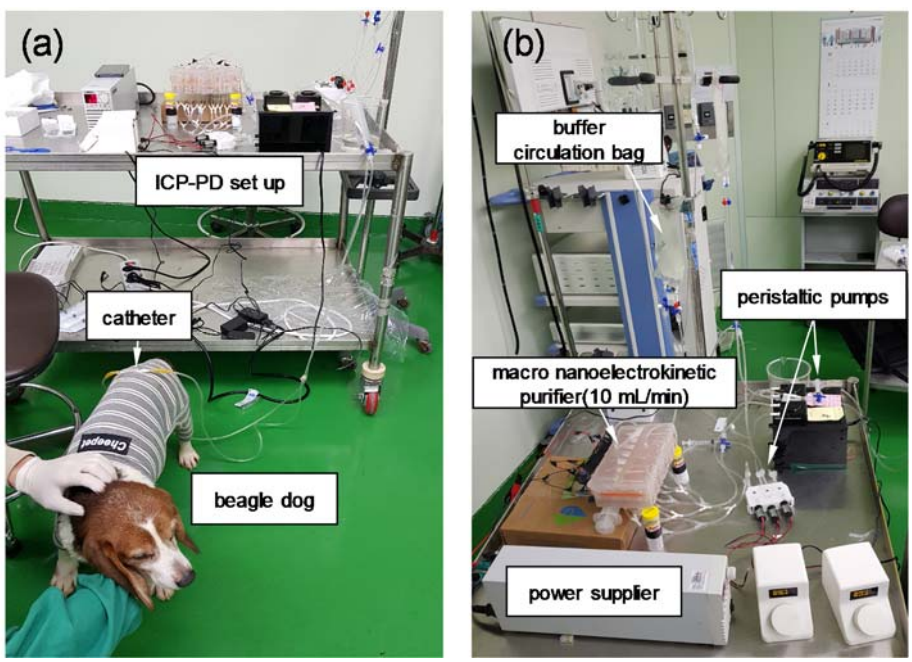

Figure 4.17. (a) An image of in-vivo closed-loop continuous nano-electrokinetic PD experiment set up and (b) specific circuit of nano-

electrokinetic-PD set up.

A closed-loop experiment for the circulation of dialysate in abdominal cavity of beagle dog was set up as shown in figure 4.16 (a). A used dialysate in abdominal cavity of the dog was withdrawn through a catheter at 10 mL/min flow rate by peristaltic pump 1, and continuously passed through the silk fibroin filter and macro nanoelectrokinetic purifier. Current and voltage changes in macro nanoelectrokinetic purifier were monitored in real time by power supplier as shown in figure 4.16 (b). Purified dialysate was withdrawn from the macro nanoelectrokinetic purifier by a peristaltic pump 2 and passed through the sensor units for monitoring concentration of urea and electrolyte ions in real time as shown in figure 4.16 (c). Finally, purified dialysate was reinjected into the abdominal cavity of the dog. This dialysate circulation is continuously repeated to purify the used dialysate in the abdominal cavity of the dog. The buffer unit corresponding to the cathodic side was implemented so as to have an independent circuit to be circulated at a flow rate of 10 mL/min by a peristaltic pump 3.

After applying regular PD treatment with dialysate of 40 cc/kg for initial 3 days, untreated 2 days, and regular PD at 60 cc/kg were applied for 5 days, a closed-loop continuous nanoelectrokinetic-PD experiment was set up as shown in figure 4.17 (a) and (b). Experiment set up was similar to that in figure 4.16.

(a)

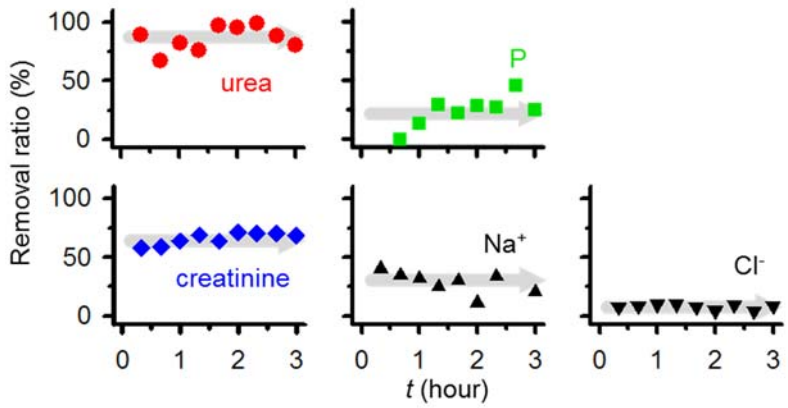

(b)

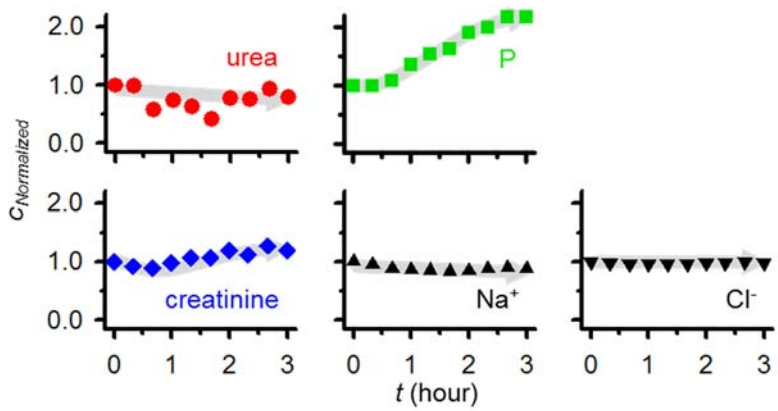

Figure 4.18. (a) Graphs of the removal ratio of the major indicators by the macro nanoelectrokinetic purifier with respect to time.

(b) Graphs of the normalized concentration of the major indicators in the abdominal cavity of the beagle dog with respect to time. The concentration of urea, Na^+ and Cl^- kept decreased, but creatinine and P increased with fluctuations because of the real-time toxin exchange process through the peritoneum.

A used dialysate in the abdominal cavity of the beagle dog was withdrawn through a catheter at 10 mL/min flow rate by a peristaltic pump, and continuously passed through the macro nanoelectrokinetic purifier. Purified dialysate was withdrawn from the macro nanoelectrokinetic purifier by a peristaltic pump. Finally, purified dialysate was reinjected into the abdominal cavity of the beagle dog. The buffer unit corresponding to the cathodic side was implemented so as to have an independent circuit to be circulated at a flow rate of 10 mL/min by a peristaltic pump. Here buffer circulation bag was utilized instead of buffer chamber.

Figure 4.18 (a) showed the removal ratio of several indicators after single-path purification over time. The removal ratio was calculated as (1-(concentration at node c)/(concentration at node b)) ×100 (%). The value was normalized by each of initial injection concentration. In the case of urea, the removal performance was stably maintained so the average removal ratio was measured at 86.4 %. In the case of creatinine, Na^+ and Cl^-, the removal ratio was also stably maintained with the average values were removal ratio of 66.1 %, 28.3 % and 7.7 %, respectively. Compared with in-vitro test experiment result, the removal ratio of Na^+ and Cl^- was similar or slightly lower, but around 30 % of creatinine was more removed due to the support from the silk-fibroin filter. On the other hand, the removal ratio of P removal rate was increased compared to the result of in-vitro experiment. The average removal ratio of P was measured at 20.3 %. P was not initially removed but started to be decomposed after an hour of operation so that the average

removal ratio was measured at 20.3 %. These results implied that the electric field was stably distributed and strong enough to decompose P in the in vivo device which was utilized in-vivo experiment.

The normalized concentrations of each species indicators in the canine abdominal cavity were plotted in Figure 4.18 (b). The concentration of urea, Na^+ and Cl^- kept decreased as expected, while that of creatinine and P kept increased with fluctuations. Since the exchange of the substance between the purified dialysate in the abdominal cavity and the blood compartment through the peritoneum actively occurs, creatinine in the blood was newly diffused into the abdominal cavity. This amount of inflow was determined by the difference in the concentration of the substance in the blood and the substance in the peritoneal fluid so that such a non-uniform concentration distribution appeared. In the meantime, the concentrations of each indicator obtained from the canine serum were analyzed as shown in Figure 4.19 (a). As the purified dialysate was continuously reinjected into the abdominal cavity, the concentrations of urea, creatinine, Na^+ and Cl^- were gradually decreased as a function of time. The concentration of P was also decreased but fluctuation level was observed possibly due to fast vortical flow by ICP [24] inducing cell lysis in the body. As a result, total toxin level in a body fluid of the beagle dog was reduced around 10 % during 3 hours of macro nanoelectrokinetic purifier operation. This critical evidence suggested that conventional PD processes could be replaced by continuous flow PD with macro nanoelectrokinetic purifier.

(a)

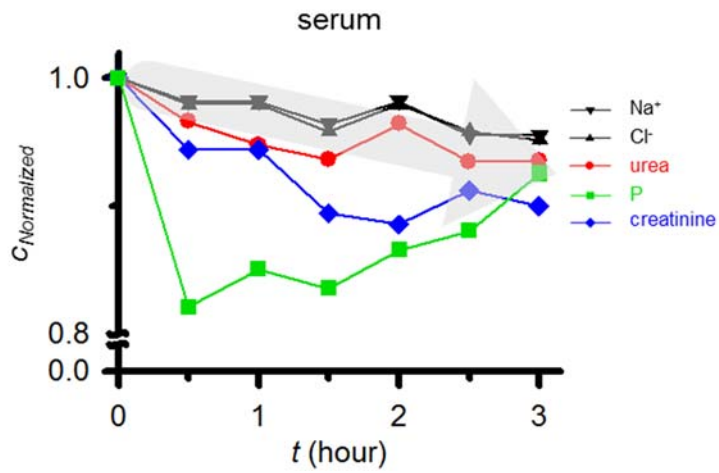

(b)

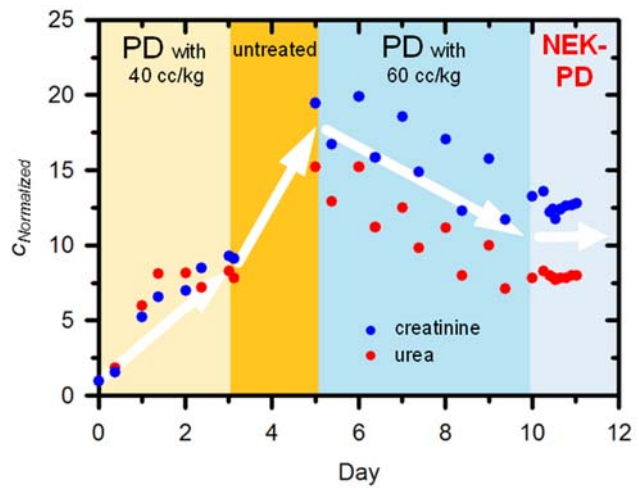

Figure 4.19. (a) Graphs of the normalized concentration of the major indicators in the serum of the beagle dog with respect to time. The concentrations of urea, creatinine, Na^+ and Cl^- were gradually decreased but P was decreased with fluctuations due to metabolism.

(b) Graphs of major toxin level changes in the beagle dog without kidneys during 12 days.

For an extreme case, both kidneys of the beagle dog were completely removed and long-term in-vivo test experiment for 12 days was conducted and the concentration of major toxin (urea and creatinine) from the canine serum was plotted as shown in Figure 4.19(b). Regular Conventional PD treatment with dialysate of 40 cc/kg was applied for initial 3 days right after the nephrectomy. Urea and creatinine continuously increased and they were explosively elevated in following 2 untreated days. Then the toxins were decreased once regular conventional PD at 60 cc/kg were applied for 5 days. After these control experiments, continuous flow nanoelectrokinetic-PD (NEK-PD) was applied to the beagle dog. See supporting information 5 for experiment images. See experimental method section for preparation of the canine model and figure 4.17 for experiment set-up images. Here silk-fibroin filter was not able to utilize since debris in a peritoneal fluid blocked the filter pores in short time. As a result, both toxins were almost maintained their initial concentration, providing a conclusion that continuous flow NEK-PD can replace regular conventional PD with the dialysate volume between 40 and 60 cc/kg. Therefore, once the nanoelectrokinetic dialysate purifier, pumps, filters, and sensors would be integrated, one can operate the system as portable artificial kidney WAK which would provide maximum convenience to the ESRD patients of end stage renal disease.

4.6 Conclusion

A nanoelectrokinetic dialysate purification device for continuous flow PD was successfully demonstrated. First, we confirmed that the most of toxic substances (urea, creatinine, Na^+, Cl^- and P) were substantially removed from the micro-nanofluidic platform. Charged substances such as Na^+ and creatinine were electrically transported through the cation selective nanoporous membrane depending on their electrophoretic mobility and electrically neutral substance such a urea was electrochemically decomposed above the threshold potentials.

To maintain these removal mechanisms in the macro-fluidic environment, we carefully designed the scaled-up devices using 3D printer with fine mesh structures and Nafion sheet. Final module is able to purify a used dialysate at 10 mL/min with over 30 % removal ratio so that toxins level in a body fluid was reduced around 10 % during 3 hours. Throughput and removal ratio would be manipulated by leveraging electric conditions and pressure field at discretion. The throughput and clearance target could also be adjusted by the number of stacked single module and electrical conditions, respectively. In-vitro experiment with closed circuit that simulated continuous flow PD treatment and in-vivo experiment with chronic renal failure canine model verified the performance of the nanoelectrokinetic purifier. Conclusively, one can expect an integrate system as WAK which would provide maximum convenience to the ESRD patients, once the nanoelectrokinetic dialysate purifier, pumps, filters, and sensors were integrated.

Chapter 5. Conclusions

While a nanofluidic device has been actively developed for a decade, lack of both amplification ratio and throughput still impeded commercial applications.

Firstly in this thesis, two types of nanofluidic preconcentrator were proposed which show a great possibility to extract highly concentrated ions and charged species in micro-nanofluidic hybrid system. Repeating each given operation steps of both types of preconcentrator effectively generated highly preconcentrated sample during the period of release time at minimum power consumption.

Secondly, the major hurdle hindered further development had been the low throughput due to microscale platform and the instability due to amplified electrokinetic field. Micro fin structure was installed near nanoporous membrane which were experimentally proven to be an appropriate remedy of such limitations. The structure would physically trap the instability which come from the scaling-up the channel dimension. While the throughput in this work was still questionable for commercial products, the presenting microstructure would play a key role for the massive parallelization even in 3-dimensional platform.

Finally, a nanoelectrokinetic dialysate purification device for continuous flow PD was successfully demonstrated. First, we confirmed that the most of toxic substances (urea, creatinine, Na^+, Cl^- and P) were substantially removed

from the micro-nanofluidic platform. Charged substances such as Na^+ and creatinine were electrically transported through the cation selective nanoporous membrane depending on their electrophoretic mobility and electrically neutral substance such a urea was electrochemically decomposed above the threshold potentials.

To maintain these removal mechanisms in the macro-fluidic environment, we carefully designed the scaled-up devices using 3D printer with fine mesh structures and Nafion sheet. Final module is able to purify a used dialysate at 10 mL/min with over 30 % removal ratio so that toxins level in a body fluid was reduced around 10 % during 3 hours. Throughput and removal ratio would be manipulated by leveraging electric conditions and pressure field at discretion. The throughput and clearance target could also be adjusted by the number of stacked single module and electrical conditions, respectively. In-vitro experiment with closed circuit that simulated continuous flow PD treatment and in-vivo experiment with chronic renal failure canine model verified the performance of the nanoelectrokinetic purifier. Conclusively, one can expect an integrate system as WAK which would provide maximum convenience to the ESRD patients, once the nanoelectrokinetic dialysate purifier, pumps, filters, and sensors were integrated.

Biblography

[1] H. v. Helmholtz, "Ueber einige Gesetze der Vertheilung elektrischer Ströme in körperlichen Leitern mit Anwendung auf die thierisch-elektrischen Versuche," *Annalen der Physik,* vol. 165, pp. 211-233, 1853.

[2] R. F. Probstein, *Physicochemical Hydrodynamics : An Introduction*: Wiley-Interscience, 1994.

[3] R. B. Schoch, J. Han, and P. Renaud, "Transport phenomena in nanofluidics," *Reviews of modern physics,* vol. 80, p. 839, 2008.

[4] S. J. Kim, S. H. Ko, K. H. Kang, and J. Han, "Direct seawater desalination by ion concentration polarization," *Nature Nanotechnology,* vol. 5, pp. 297-301, 2010.

[5] H. Strathmann, "Electrodialysis, a mature technology with a multitude of new applications," *Desalination,* vol. 264, pp. 268-288, 2010.

[6] J. Wood, J. Gifford, J. Arba, and M. Shaw, "Production of ultrapure water by continuous electrodeionization," *Desalination,* vol. 250, pp. 973-976, 2010.

[7] M. A. Anderson, A. L. Cudero, and J. Palma, "Capacitive deionization as an electrochemical means of saving energy and delivering clean water. Comparison to present desalination practices: Will it compete?," *Electrochimica Acta,* vol. 55, pp. 3845-3856, 2010.

[8] V. V. Nikonenko, A. V. Kovalenko, M. K. Urtenov, N. D. Pismenskaya, J. Han, P. Sistat*, et al.*, "Desalination at overlimiting currents: State-of-the-art and perspectives," *Desalination,* vol. 342, pp. 85-106, Jun 2014.

[9] T. Humplik, J. Lee, S. O'hern, B. Fellman, M. Baig, S. Hassan*, et al.*, "Nanostructured materials for water desalination," *Nanotechnology,* vol. 22, p. 292001, 2011.

[10] F. Maletzki, H.-W. Rosler, and E. Staude, "Ion transfer across electrodialysis membranes in the overlimiting current range stationary voltage current characteristics and current noise power spectra under different conditions of free convection," *Journal of membrane science,* vol. 71, pp. 105-116, 1992.

[11] P. K. Narayanan, S. K. Thampy, N. J. Dave, D. K. Chauhan, B. S. Makwana, S. K. Adhikary*, et al.*, "Performance of the first sea water electrodialysis desalination plant in india," *Desalination,* vol. 84, pp. 201-211, 1991.

[12] J.-H. Lee, W.-S. Bae, and J.-H. Choi, "Electrode reactions and adsorption/desorption performance related to the applied potential in a capacitive deionization process," *Desalination,* vol. 258, pp. 159-163, 2010.

[13] A. Subramani, M. Badruzzaman, J. Oppenheimer, and J. G. Jacangelo, "Energy minimization strategies and renewable energy utilization for desalination: A review," *Water Research,* vol. 45, pp. 1907-1920, Feb 2011.

[14] S. J. Kim, Y.-C. Wang, J. H. Lee, H. Jang, and J. Han, "Concentration Polarization and Nonlinear Electrokinetic Flow near Nanofluidic Channel," *Physical Review Letters,* vol. 99, p. 044501, 27 Jul 2007 2007.

[15] S. H. Ko, Y. A. Song, S. J. Kim, M. Kim, J. Han, and K. H. Kang, "Nanofluidic preconcentration device in a straight microchannel using ion concentration polarization," *Lab on a Chip,* vol. 12, pp. 4472-4482, 2012.

[16] R. Kwak, S. J. Kim, and J. Han, "Continuous-flow biomolecule and cell concentrator by ion concentration polarization," *Analytical Chemistry,* vol. 83, pp. 7348-7355, 2011.

[17] T. A. Zangle, A. Mani, and J. G. Santiago, "Theory and experiments of concentration polarization and ion focusing at microchannel and nanochannel interfaces," *Chemical Society Reviews,* vol. 39, pp. 1014-1035, 2010.

[18] W. Kim, K. Kim, H. Lee, Y. S. Kim, J. C. Lee, G. Y. Sung*, et al.*, "Nanoelectrokinetic purification device for a continuous peritoneal dialysate recycler," in *2017 IEEE 30th International Conference on Micro Electro Mechanical Systems (MEMS)*, 2017, pp. 319-322.

[19] G. Yossifon and H. C. Chang, "Changing nanoslot ion flux with a dynamic nanocolloid ion-selective filter: Secondary overlimiting currents due to nanocolloid-nanoslot interaction," *Physical Review E,* vol. 81, p. 066317, Jun 2010.

[20] C.-H. Chen, H. Lin, S. K. Lele, and J. G. Santiago, "Convective and absolute electrokinetic instability with conductivity gradients," *Journal of Fluid Mechanics,* vol. 524, pp. 263-303, 2005.

[21] J. D. Posner and J. G. Santiago, "Convective instability of electrokinetic flows in a cross-shaped microchannel," *Journal of Fluid Mechanics,* vol. 555, pp. 1-42, 2006.

[22] C. L. Druzgalski, M. B. Andersen, and A. Mani, "Direct numerical simulation of electroconvective instability and hydrodynamic chaos near an ion-selective surface," *Physics of Fluids,* vol. 25, p. 110804, Nov 2013.

[23] S. M. Rubinstein, G. Manukyan, A. Staicu, I. Rubinstein, B. Zaltzman, R. G. H. Lammertink*, et al.*, "Direct Observation of a Nonequilibrium Electro-Osmotic Instability " *Physical Review Letters,* vol. 101, p. 236101, 2008.

[24] S. J. Kim, S. H. Ko, R. Kwak, J. D. Posner, K. H. Kang, and J. Han, "Multi-vortical flow inducing electrokinetic instability in ion concentration polarization layer," *Nanoscale,* vol. 4, pp. 7406-7410, 2012.

[25] M. A. Unger, H.-P. Chou, T. Thorsen, A. Scherer, and S. R. Quake, "Monolithic microfabricated valves and pumps by multilayer soft lithography," *Science,* vol. 288, pp. 113-116, 2000.

[26] B. S. Reto, H. Jongyoon, and R. Philippe, "Transport phenomena in nanofluidics," *Reviews of Modern Physics,* vol. 80, p. 839, 2008.

[27] R. H. Austin, "Nanofluidics: A fork in the nano-road," *Nature Nanotechnology,* vol. 2, pp. 79-80, 2007.

[28] J. C. T. Eijkel and A. van den Berg, "Nanofluidics: what is it and what can we expect from it?," *Microfluidics and Nanofluidics,* vol. 1, pp. 249-267, 2005.

[29] Q. Pu, J. Yun, H. Temkin, and S. Liu, "Ion-Enrichment and Ion-Depletion Effect of Nanochannel Structures," *Nano Letters,* vol. 4, pp. 1099-1103, 2004.

[30] S.-H. Lee, H. Lee, T. Jin, S. Park, B. J. Yoon, G. Y. Sung*, et al.*, "Sub-10 nm transparent all-around-gated ambipolar ionic field effect transistor," *Nanoscale,* vol. 7, pp. 936-946, 2015.

[31] S. J. Kim, Y.-A. Song, and J. Han, "Nanofluidic concentration devices for biomolecules utilizing ion concentration polarization: theory, fabrication, and application," *Chemical Society Reviews,* vol. 39, pp. 912-922, 2010.

[32] K. A. Mauritz and R. B. Moore, "State of understanding of Nafion," *Chemical Reviews,* vol. 104, pp. 4535-4585, 2004.

[33] I. Cho, W. Kim, J. Kim, H.-Y. Kim, H. Lee, and S. J. Kim, "Non-Negligible Diffusio-Osmosis Inside an Ion Concentration Polarization Layer," *Physical Review Letters,* vol. 116, p. 254501, 06/20/ 2016.

[34] S. Nam, I. Cho, J. Heo, G. Lim, M. Z. Bazant, D. J. Moon*, et al.*, "Experimental Verification of Overlimiting Current by Surface Conduction and Electro-Osmotic Flow in Microchannels," *Physical Review Letters,* vol. 114, p.

114501, 2015.

[35] E. V. Dydek, B. Zaltzman, I. Rubinstein, D. S. Deng, A. Mani, and M. Z. Bazant, "Overlimiting Current in a Microchannel," *Physical Review Letters,* vol. 107, p. 118301, 2011.

[36] D. Deng, E. V. Dydek, J.-H. Han, S. Schlumpberger, A. Mani, B. Zaltzman*, et al.*, "Overlimiting Current and Shock Electrodialysis in Porous Media," *Langmuir,* vol. 29, pp. 16167-16177, 2013.

[37] S. M. Davidson, M. B. Andersen, and A. Mani, "Chaotic Induced-Charge Electro-Osmosis," *Physical Review Letters,* vol. 112, p. 128302, 2014.

[38] T. Pundik, I. Rubinstein, and B. Zaltzman, "Bulk electroconvection in electrolyte," *Physical Review E,* vol. 72, p. 061502, 2005.

[39] I. Rubinstein and B. Zaltzman, "Electroconvective instability in concentration polarization and nonequilibrium electro-osmotic slip," *Physical Review E (Statistical, Nonlinear, and Soft Matter Physics),* vol. 72, p. 011505, 2005.

[40] H. C. Chang, G. Yossifon, and E. A. Demekhin, "Nanoscale Electrokinetics and Microvortices: How Microhydrodynamics Affects Nanofluidic Ion Flux," *Annual Review of Fluid Mechanics,* vol. 44, pp. 401-426, 2012.

[41] R. Kwak, G. F. Guan, W. K. Peng, and J. Y. Han, "Microscale electrodialysis: Concentration profiling and vortex visualization," *Desalination,* vol. 308, pp. 138-146, Jan 2013.

[42] S. Park, Y. Jung, S. Y. Son, I. Cho, Y. Cho, H. Lee*, et al.*, "Capillarity ion concentration polarization as spontaneous desalting mechanism," *Nat Commun,* vol. 7, p. 11223, 04/01/online 2016.

[43] J. Choi, K. Huh, D. J. Moon, H. Lee, S. Y. Son, K. Kim*, et al.*, "Selective preconcentration and online collection of charged molecules using ion concentration polarization," *RSC Advances,* vol. 5, pp. 66178-66184, 2015.

[44] Y. Oh, H. Lee, S. Y. Son, S. J. Kim, and P. Kim, "Capillarity ion concentration polarization for spontaneous biomolecular preconcentration mechanism," *Biomicrofluidics,* vol. 10, p. 014102, 2016.

[45] S. H. Ko, S. J. Kim, L. Cheow, L. D. Li, K. H. Kang, and J. Han, "Massively-Parallel Concentration Device for Multiplexed Immunoassays," *Lab on a Chip,* vol. 11, pp. 1351-1358, 2011.

[46] K. N. Knust, D. Hlushkou, R. K. Anand, U. Tallarek, and R. M. Crooks, "Electrochemically Mediated Seawater Desalination," *Angewandte chemie International Edition,* vol. 52, pp. 8107-8110, 2013.

[47] C.-H. Chen, A. Sakar, Y.-A. Song, M. A. Miller, S. J. Kim, L. G. Griffith*, et al.*, "Enhancing Protease Activity Assay in Droplet-Based Microfluidics Using a Biomolecule Concentrator," *Journal of the American Chemical Society,* vol. 133, pp. 10368-10371, 2011.

[48] B. Zaltzman and I. Rubinstein, "Electro-osmotic slip and electroconvective instability," *Journal of Fluid Mechanics,* vol. 579, pp. 173-226, 2007.

[49] S. J. Kim, L. Li, and J. Han, "Amplified Electrokinetic Response by Concentration Polarization near Nanofluidic Channel," *Langmuir,* vol. 25, pp. 7759-7765, 2009.

[50] R. Dhopeshwarkar, R. M. Crooks, D. Hlushkou, and U. Tallarek, "Transient Effects on Microchannel Electrokinetic Filtering with an Ion-Permselective Membrane," *Analytical Chemistry,* vol. 80, pp. 1039-1048, 2008.

[51] I. Cho, G. Sung, and S. J. Kim, "Overlimiting Current Through Ion Concentration Polarization Layer: Hydrodynamic Convection Effects," *Nanoscale,* vol. 6, pp. 4620-4626, 2014.

[52] Y.-C. Wang, A. L. Stevens, and J. Han, "Million-fold Preconcentration of Proteins and Peptides by Nanofluidic Filter," *Analytical Chemistry,* vol. 77, pp. 4293-4299, 2005.

[53] B. Jung, R. Bharadwaj, and J. G. Santiago, "On-chip Millionfold Sample Stacking Using Transient Isotachophoresis," *Analytical Chemistry,* vol. 78, pp. 2319-2327, 2006.

[54] D. Janasek, M. Schilling, J. Franzke, and A. Manz, "Isotachophoresis in Free-Flow Using a Miniaturized Device," *Analytical Chemistry,* vol. 78, pp. 3815-3819, 2006.

[55] N. P. Beard, C.-X. Zhang, and A. J. deMello, "In-column field-amplified sample stacking of biogenic amines on microfabricated ellectrophoresis devices " *Electrophoresis,* vol. 24, pp. 732-739, 2003.

[56] B. Jung, R. Bharadwaj, and J. G. Santiago, "Thousandfold signal increase using field-amplified sample stacking for on-chip electrophoresis," *ELECTROPHORESIS,* vol. 24, pp. 3476-3483, 2003.

[57] Y.-C. Wang and J. Han, "Pre-binding dynamic range and sensitivity enhancement for immuno-sensors using nanofluidic preconcentrator," *Lab on a Chip,* vol. 8, pp. 392-394, 2008.

[58] "u.s. Renal Data System, USRDS 2010 Annual data report: atlas of chronic kidney disease and end-stage renal disease in the United States," *National Institutes of Health & National Institute of Diabetes and Digestive and*

Kidney Diseases, 2010.

[59] V. Jha, G. Garcia-Garcia, K. Iseki, Z. Li, S. Naicker, B. Plattner*, et al.*, "Chronic kidney disease: global dimension and perspectives," *The Lancet,* vol. 382, pp. 260-272, 2013.

[60] R. Saran, B. Robinson, K. C. Abbott, L. Y. Agodoa, P. Albertus, J. Ayanian*, et al.*, "US renal data system 2016 annual data report: epidemiology of kidney disease in the United States," *American journal of kidney diseases,* vol. 69, pp. A7-A8, 2017.

[61] C. Medin, C. G. Elinder, B. Hylander, B. Blom, and H. Wilczek, "Survival of patients who have been on a waiting list for renal transplantation," *Nephrology Dialysis Transplantation,* vol. 15, pp. 701-704, 2000.

[62] F. K. Port, R. A. Wolfe, E. A. Mauger, D. P. Berling, and K. Jiang, "Comparison of survival probabilities for dialysis patients vs cadaveric renal transplant recipients," *Jama,* vol. 270, pp. 1339-1343, 1993.

[63] R. A. Wolfe, V. B. Ashby, E. L. Milford, A. O. Ojo, R. E. Ettenger, L. Y. Agodoa*, et al.*, "Comparison of mortality in all patients on dialysis, patients on dialysis awaiting transplantation, and recipients of a first cadaveric transplant," *New England Journal of Medicine,* vol. 341, pp. 1725-1730, 1999.

[64] R. Jofre, J. M. López-Gómez, F. Moreno, D. Sanz-Guajardo, and F. Valderrábano, "Changes in quality of life after renal transplantation," *American Journal of Kidney Diseases,* vol. 32, pp. 93-100, 1998.

[65] A. Laupacis, P. Keown, N. Pus, H. Krueger, B. Ferguson, C. Wong*, et al.*, "A study of the quality of life and cost-utility of renal transplantation," *Kidney international,* vol. 50, pp. 235-242, 1996.

[66] A. J. Lee, C. L. Morgan, P. Conway, and C. J. Currie, "Characterisation and comparison of health-related quality of life for patients with renal failure," *Current medical research and opinion,* vol. 21, pp. 1777-1783, 2005.

[67] A. Lee, C. Gudex, J. V. Povlsen, B. Bonnevie, and C. P. Nielsen, "Patients' views regarding choice of dialysis modality," *Nephrology Dialysis Transplantation,* vol. 23, pp. 3953-3959, 2008.

[68] J. Little, A. Irwin, T. Marshall, H. Rayner, and S. Smith, "Predicting a patient's choice of dialysis modality: experience in a United Kingdom renal department," *American journal of kidney diseases,* vol. 37, pp. 981-986, 2001.

[69] R. L. Morton, P. Snelling, A. C. Webster, J. Rose, R. Masterson, D. W. Johnson*,*

et al., "Dialysis modality preference of patients with CKD and family caregivers: a discrete-choice study," *American Journal of Kidney Diseases,* vol. 60, pp. 102-111, 2012.

[70] "II. NKF-K/DOQI Clinical Practice Guidelines for Peritoneal Dialysis Adequacy: Update 2000," *American Journal of Kidney Diseases,* vol. 37, pp. S65-S136, 2001/01/01/ 2001.

[71] N. Aslam, J. Bernardini, L. Fried, R. Burr, and B. Piraino, "Comparison of infectious complications between incident hemodialysis and peritoneal dialysis patients," *Clinical Journal of the American Society of Nephrology,* vol. 1, pp. 1226-1233, 2006.

[72] J. G. Heaf, H. Løkkegaard, and M. Madsen, "Initial survival advantage of peritoneal dialysis relative to haemodialysis," *Nephrology Dialysis Transplantation,* vol. 17, pp. 112-117, 2002.

[73] J. C. Korevaar, G. Feith, F. W. Dekker, J. G. Van Manen, E. W. Boeschoten, P. M. Bossuyt*, et al.*, "Effect of starting with hemodialysis compared with peritoneal dialysis in patients new on dialysis treatment: a randomized controlled trial," *Kidney international,* vol. 64, pp. 2222-2228, 2003.

[74] M. P. Fontan, A. Rodriguez-Carmona, T. G. Falcon, J. Moncalian, J. Oliver, and F. Valdes, "Renal transplantation in patients undergoing chronic peritoneal dialysis," *Peritoneal dialysis international,* vol. 16, pp. 48-51, 1996.

[75] R. Vanholder, P. Heering, A. Van Loo, W. Van Biesen, M.-C. Lambert, U. Hesse*, et al.*, "Reduced incidence of acute renal graft failure in patients treated with peritoneal dialysis compared with hemodialysis," *American Journal of Kidney Diseases,* vol. 33, pp. 934-940, 1999.

[76] V. Gura, M. B. Rivara, S. Bieber, R. Munshi, N. C. Smith, L. Linke*, et al.*, "A wearable artificial kidney for patients with end-stage renal disease," *JCI insight,* vol. 1, 2016.

[77] A. Davenport, "Dialysis: A wearable dialysis device: the first step to continuous therapy," *Nature Reviews Nephrology,* vol. 12, p. 512, 2016.

[78] J. Glater, "The early history of reverse osmosis membrane development," *Desalination,* vol. 117, pp. 297-309, 1998.

[79] B. Kim, R. Kwak, H. J. Kwon, V. S. Pham, M. Kim, B. Al-Anzi*, et al.*, "Purification of High Salinity Brine by Multi-Stage Ion Concentration Polarization Desalination," *Scientific Reports,* vol. 6, p. 31850, 08/22/online 2016.

[80] S. Choi, B. Kim, and J. Han, "Integrated pretreatment and desalination by electrocoagulation (EC)–ion concentration polarization (ICP) hybrid," *Lab on a Chip,* vol. 17, pp. 2076-2084, 2017.

[81] K. Kim, W. Kim, H. Lee, and S. J. Kim, "Stabilization of ion concentration polarization layer using micro fin structure for high-throughput applications," *Nanoscale,* vol. 9, pp. 3466-3475, 2017.

[82] W. Kim, S. Park, K. Kim, and S. J. Kim, "Experimental verification of simultaneous desalting and molecular preconcentration by ion concentration polarization," *Lab on a Chip,* vol. 17, pp. 3841-3850, 2017.

[83] S. HA, S. AD, and A. A, "Engineering flows in small devices: Microfluidics toward a lab-on-a-chip " *Annual Review of Fluid Mechanics,* vol. 36, pp. 381-411, 2004.

[84] S. J. Kim and J. Han, "Self-Sealed Vertical Polymeric Nanoporous Junctions for High-Throughput Nanofluidic Applications," *Analytical Chemistry,* vol. 80, pp. 3507-3511, 2008.

[85] I. Rubinstein and B. Zaltzman, "Electro-convective versus electroosmotic instability in concentration polarization," *Advances in Colloid and Interface Science,* vol. 134-35, pp. 190-200, Oct 2007.

[86] P. Kim, S. J. Kim, K.-Y. Suh, and J. Han, "Stabilization of ion concentration polarization using a heterogeneous nanoporous junction," *Nano Letters,* vol. 10, pp. 16-23, 2010.

[87] I. Rubinstein and B. Zaltzman, "Equilibrium Electroconvective Instability," *Physical Review Letters,* vol. 114, p. 114502, 03/16/ 2015.

[88] S. J. Yao, S. K. Wolfson Jun, B. K. Ahn, and C. C. Liu, "Anodic Oxidation of Urea and an Electrochemical Approach to De-ureation," *Nature,* vol. 241, p. 471, 02/16/online 1973.

[89] W. Simka, J. Piotrowski, and G. Nawrat, "Influence of anode material on electrochemical decomposition of urea," *Electrochimica Acta,* vol. 52, pp. 5696-5703, 2007/05/10/ 2007.

[90] M. Wester, F. Simonis, N. Lachkar, K. Wodzig Will, J. Meuwissen Frank, P. Kooman Jeroen*, et al.*, "Removal of Urea in a Wearable Dialysis Device: A Reappraisal of Electro-Oxidation," *Artificial Organs,* vol. 38, pp. 998-1006, 2014.

[91] A. I. Arieff, "Dialysis disequilibrium syndrome: current concepts on pathogenesis and prevention," *Kidney international,* vol. 45, pp. 629-635, 1994.

[92] K. Kjeldsen, "Hypokalemia and sudden cardiac death," *Experimental & Clinical Cardiology,* vol. 15, p. e96, 2010.

[93] J. H. Lee, Y.-A. Song, and J. Han, "Multiplexed Proteomic Sample Preconcentration Device Using Surface-Patterned Ion-Selective Membrane " *Lab on a Chip,* vol. 8, pp. 596 - 601, 2008.

[94] S. Y. Son, S. Lee, H. Lee, and S. J. Kim, "Engineered nanofluidic preconcentration devices by ion concentration polarization," *BioChip Journal,* vol. 10, pp. 251-261, 2016.

초 록

근래의 이온 선택적 투과막과 나노스케일 공정의 발전과 맞물려, 정수/농축을 목적으로 하는 다양한 전기수력학적 수처리 방법이 개발되고 있다. 그 중 이온농도분극(Ion concentration polarization) 현상은 나노스케일 전기수력학의 학문적 기반과 새로운 응용분야를 성장시킬 후보로 주목 받고 있다. 하지만 아직 이온농도분극 현상을 활용한 효과적인 플랫폼이 충분치 않으며, 마이크로/나노 시스템의 필연적인 한계인 낮은 처리용량을 극복하지 못하고 있다. 본 학위논문에서는 마이크로 유체역학 장치를 접목시킨 이온농도분극 현상 기반의 새로운 정수/농축 플랫폼을 개발하고, 현상이 발생하는 나노막 근처에 마이크로 구조물을 설치함으로써 이온농도분극 현상 기반 장치의 전기적 특성을 향상시킴과 동시에 처리용량을 증가시켰다. 최종적으로, 인공 신장 시스템을 위한 전기수력학 정수 장치를 개발하였다.

첫째, 액적 발생기와 공압 밸브를 접목한 ICP 현상 기반의 마이크로/나노 유체역학 장치를 개발하였다. 이온농도분극 현상의 가장 흥미로운 특징 중 하나는 전하를 가진 모든 입자들이 이온농도분극현상 영역의 경계에 모인다는 점이며, 이 때 경계의 농축비를 수 분에 10,000 배까지 증폭할 수 있다. 샘플이 고농도로 농축된 플러그의 확산을 막기 위하여 액적 발생기를 도입하였으며, 고농축 플러그를 액적에 가둠으로써 농도의 손실 없이 추출할 수 있다. 이 때 전압/전류, 유량, 농축 시간 등을 조절하여 원하는 농축비의 플러그를 얻을 수 있다. 추가적으로, 이온농도분극 현상을 이용한 연속작동 방식의 농축 장치에 공압 밸브를 결합하였다. 고농도로 농축된 플러그를 짧은 시간(<100 ms) 동안 밸브 조작을 통해 개방된 특정 분지로 내보냄으로써 농축액을 연속적으로 얻을 수

있는 방식이다. 농축비 조절 방법은 액적 발생기를 접목한 농축 장치와 거의 동일하며, 100배 이상의 농축비를 얻었다.

둘째, 수백 마이크로미터 이상의 채널을 갖는 이온농도분극 현상 장치에 지느러미 형태의 마이크로 구조물을 설치하여 안정적인 현상 발생과 성능 유지를 확인하였다. 이 구조는 이온농도분극 현상 영역에서 발생하는 불안정한 와류를 억제하여 전기삼투 유동에 의한 이온 전달을 우세하도록 환경을 바꾸므로, 밀리미터 스케일 이상의 장치에서도 이온농도분극 현상을 안정적으로 발생/유지할 수 있도록 한다. 수식 해석과 수치 해석 후에 구조물을 설계하였다. 마지막으로, 앞서 언급한 액적발생기와 융합된 이온농도분극 현상 기반의 농축 장치와 연속 방식의 정수 장치에 이 구조를 설치함으로써 밀리미터 이상의 채널 크기를 갖는 장치에서도 이온농도분극 현상이 안정적으로 발생/유지하여 장치가 문제 없이 작동하는 것을 보였다.

최종적으로, 인공 신장 시스템을 위한 고처리 용량의 전기수력학 정수 장치를 개발하였다. 복막 투석(Peritoneal dialysis) 기반의 착용형 인공신장(Wearable artificial kidney)이며, 휴대용이고 정수 정도를 자동으로 조정하므로 기존의 복막투석/혈액투석(hemodialysis)로 치료받는 말기 신부전증(End stage renal disease) 환자의 시간/공간적 제약을 해방할 것으로 기대한다. 이온농도분극 현상 기반의 나노전기수력학 장치는 이온부터 마이크로미터 크기의 입자들까지 모두 분리할 수 있으므로 휴대용 정수 장치로써의 개발 가능성에 많은 관심이 모아졌다. 이 연구에서는, 이온농도분극 현상 기반의 나노전기수력학 장치를 휴대용 복막 투석 재생기로 개발함으로써 기존의 복막투석의 단점들을 극복하고자 한다. 우선, 나노전기수력학을 이용한 복막 투석액의 재생 메커니즘을 마이크로-나노 플랫폼에서 확인하였다. 전하를 갖지 않는 요독 물질인 유레아(urea)는 전기화학적 반응을 통하여 99%이상 무독성 기체로 분해되었으며, 양전하를

갖는 요독 물질인 크레아티닌(creatinine)은 나노막을 통한 이동현상에 의하여 40%이상 제거되었다. 그리고 분당 10 mL/min을 처리할 수 있는 이 장치의 내부는 특정 구조물로 마이크로-나노 유체역학적 환경이 조성되어 연속적으로 복막 투석액을 정수할 수 있도록 제작되었다. *In-vitro* 실험과 *in-vivo* 실험을 통하여 장치의 작동 여부를 테스트하였고, 최종적으로 실험견 혈액 내의 요독 물질이 3시간동안 10% 정도 감소한 것을 확인하였다. 개발된 착용형 인공신장 시스템을 통하여 말기 신부전증 환자들의 삶의 질을 높일 수 있을 것으로 기대한다.

주요어 : 마이크로/나노 유체역학, 전기수력학, 이온농도분극 현상, 불안정성 억제, 수처리용량 증대, 복막 투석액 재생기

학 번 : 2013-20749